Monthly Notices of the ROYAL ASTRONOMICAL SOCIETY
MNRAS **457,** 3200–3218 (2016) doi:10.1093/mnras/stw188

Strong bimodality in the host halo mass of central galaxies from galaxy–galaxy lensing

Rachel Mandelbaum,[1⋆] Wenting Wang,[2] Ying Zu,[1] Simon White,[3] Bruno Henriques[3,4] and Surhud More[5]

[1]*McWilliams Center for Cosmology, Department of Physics, Carnegie Mellon University, Pittsburgh, PA 15213, USA*
[2]*Institute for Computational Cosmology, University of Durham, South Road, Durham DH1 3LE, UK*
[3]*Max Planck Institut fur Astrophysik, Karl-Schwarzschild-Str. 1, D-85741 Garching b. München, Germany*
[4]*Institute for Astronomy, Department of Physics, ETH Zurich, CH-8093 Zurich, Switzerland*
[5]*Kavli Institute for the Physics and Mathematics of the Universe (WPI), UTIAS, The University of Tokyo, Chiba 277-8583, Japan*

Accepted 2016 January 19. Received 2016 January 14; in original form 2015 September 22

ABSTRACT

We use galaxy–galaxy lensing to study the dark matter haloes surrounding a sample of locally brightest galaxies (LBGs) selected from the Sloan Digital Sky Survey. We measure mean halo mass as a function of the stellar mass and colour of the central galaxy. Mock catalogues constructed from semi-analytic galaxy formation simulations demonstrate that most LBGs are the central objects of their haloes, greatly reducing interpretation uncertainties due to satellite contributions to the lensing signal. Over the full stellar mass range, $10.3 < \log[M_*/\mathrm{M}_\odot] < 11.6$, we find that passive central galaxies have haloes that are at least twice as massive as those of star-forming objects of the same stellar mass. The significance of this effect exceeds 3σ for $\log[M_*/\mathrm{M}_\odot] > 10.7$. Tests using the mock catalogues and on the data themselves clarify the effects of LBG selection and show that it cannot artificially induce a systematic dependence of halo mass on LBG colour. The bimodality in halo mass at fixed stellar mass is reproduced by the astrophysical model underlying our mock catalogue, but the sign of the effect is inconsistent with recent, nearly parameter-free age-matching models. The sign and magnitude of the effect can, however, be reproduced by halo occupation distribution models with a simple (few-parameter) prescription for type dependence.

Key words: gravitational lensing: weak – galaxies: haloes – galaxies: stellar content – cosmology: observations.

1 INTRODUCTION

The relationship between the stellar mass in galaxies and the mass of their underlying dark matter haloes is a fundamental ingredient in any theory of galaxy formation and evolution. This relationship has been inferred using multiple observational techniques, each with different interpretation difficulties. These include abundance matching (e.g. Behroozi, Conroy & Wechsler 2010; Guo et al. 2010; Moster et al. 2010), galaxy clustering (e.g. Zehavi et al. 2005, 2011; White et al. 2011; Coupon et al. 2012; Parejko et al. 2013) and satellite kinematics (e.g. Conroy et al. 2007; More et al. 2011; Wojtak & Mamon 2013). Galaxy–galaxy lensing (e.g. Hoekstra, Yee & Gladders 2004; Heymans et al. 2006; Mandelbaum et al. 2006; Velander et al. 2014; Han et al. 2015; Hudson et al. 2015; Miyatake et al. 2015; van Uitert et al. 2015) exploits the weak shape distortions of distant galaxies due to the mass in nearby foreground galaxies, and therefore has the unique advantage of being directly sensitive to dark matter halo masses. However, as for galaxy clustering, the interpretation of the results can be complicated due to the different lensing profiles of central and satellite galaxies (the latter of which include a contribution from their host dark matter halo); this is also the case when combining lensing with other measurements (e.g. Cacciato et al. 2009; Leauthaud et al. 2012a; Cacciato et al. 2013; Coupon et al. 2015; More et al. 2015; Zu & Mandelbaum 2015b).

Galaxies are often classified as passive or active,[1] where passive galaxies typically have a red rest-frame colour indicative of a paucity of recent star formation, and active galaxies have bluer colours indicating recent and/or ongoing star formation. They also exhibit morphological differences and variations in their distributions with respect to the local density (with passive galaxies more

⋆ E-mail: rmandelb@andrew.cmu.edu

[1] Throughout this work, we use 'passive' versus 'active' to indicate galaxy types, and 'red' versus 'blue' to indicate rest-frame colour-selected samples (our observational proxies for passive versus active galaxies).

prevalent in high-density environments). It is natural to ask whether these two classes of galaxies, which apparently have rather different star formation histories, also have different relationships between stellar and halo mass. Unfortunately, the answer to this question is observationally unclear, with results pointing to differences between passive and active galaxies (Hoekstra et al. 2005; Mandelbaum et al. 2006; More et al. 2011; Wang & White 2012; Tinker et al. 2013; Velander et al. 2014; Hudson et al. 2015; Schaye et al. 2015), but often with quite large statistical or systematic uncertainties that can make it difficult to draw a definitive conclusion, especially at lower mass.

The relationship between stellar and halo mass can also be explored using simulation and/or galaxy modelling techniques. For example, semi-analytic models (SAMs) applied to subhalo catalogues from *N*-body simulations (as early as Kauffmann, Nusser & Steinmetz 1997; see Guo et al. 2011; Benson 2012 for more recent examples) and hydrodynamic simulations (e.g. Vogelsberger et al. 2014; Khandai et al. 2015; Schaye et al. 2015) predict a potentially quite complicated and physically based relation between the galaxies and their dark matter haloes, including a properly self-consistent treatment of the time evolution of this relationship. In both cases, there are parameters that must be tuned to match observations. For SAMs, these are explicit parameters of the semi-analytic model, while for hydrodynamic simulations, they model subgrid physics unresolved by the simulation, and again must be tuned by hand. Both methods are usually calibrated to match a subset of the interesting properties of galaxies in real data (e.g. mass functions), and then tested against different properties (e.g. clustering or evolution). In contrast, the age-matching technique (Hearin & Watson 2013; Hearin et al. 2014) can also be applied to catalogues from an *N*-body simulation, and assumes (rather than predicting) a particular relationship between the masses and ages of galaxies and those of their haloes in order to populate the haloes with galaxies.

The various theoretical frameworks mentioned above take different approaches to the issue of galaxy type dependence. Observational guidance on the colour dependence of the relation between stellar and halo mass using a simple and unambiguous measurement with minimal modelling assumptions may therefore be used to distinguish between these models. In this paper, we use a data set consisting of locally brightest galaxies (LBGs; Planck Collaboration XI 2013 and Anderson et al. 2015) in the Sloan Digital Sky Survey (SDSS) as a sample of central galaxies, classify them as passive or active based on rest-frame colours, and use weak gravitational lensing to estimate their average halo mass as a function of their stellar masses. We also present evidence that this LBG data set is a relatively fair sample of central galaxies, and use mock catalogues to correct for biases resulting from the selection method and our way of interpreting the weak lensing measurements in terms of a halo mass. The use of LBGs thus reduces sensitivity to the separation between central and satellite contributions, which is the primary source of model dependence when interpreting galaxy–galaxy lensing measurements, and we are left with a simple and direct measurement of halo masses. Wang et al. (2016) carry out a thorough exploration of how SAM-based catalogues capture the observed lensing properties of these LBGs, considering multiple cosmological models and SAMs; in this work, we use the mock catalogue that *best* reproduces the observed properties of LBGs to interpret our measurements.

The outline of this paper is as follows. In Section 2, we describe the data set used for the measurements, and in Section 4 we describe the measurements made and how they are interpreted. Section 3 includes a description of the mock catalogues used to validate the measurement method, and the result of that validation. We present our results and compare with previous work in Section 5, and discuss the implications for galaxy formation and evolution in Section 6.

All measurements made in this paper use a flat Λ cold dark matter (ΛCDM) model with $\Omega_{\rm m} = 0.315$ in accordance with the 2013 *Planck* results in Planck Collaboration XVI (2014), and stellar mass estimates are calculated in $\mathrm{M}_{\odot}$ using $h = 0.673$ as in that work. This choice was made to conform with the cosmological parameters in the mock galaxy catalogue used to validate our measurement procedure.

2 DATA

All data used in this paper came from the SDSS I/II. The SDSS I (York et al. 2000) and II surveys imaged roughly π sr of the sky, and followed up approximately one million of the detected objects spectroscopically (Eisenstein et al. 2001; Richards et al. 2002; Strauss et al. 2002). The imaging was carried out by drift-scanning the sky in photometric conditions (Hogg et al. 2001; Ivezić et al. 2004), in five bands (*ugriz*; Fukugita et al. 1996; Smith et al. 2002) using a specially designed wide-field camera (Gunn et al. 1998). These imaging data were used to create the catalogues that we use in this paper. All of the data were processed by completely automated pipelines that detect and measure photometric properties of objects, and astrometrically calibrate the data (Lupton et al. 2001; Pier et al. 2003; Tucker et al. 2006). The SDSS-I/II imaging surveys were completed with a seventh data release (Abazajian et al. 2009), from which the LBG sample described in Section 2.1 originates. The source catalogue described in Section 2.2 uses an improved data reduction pipeline that was part of the eighth data release, from SDSS-III (Aihara et al. 2011) and an improved photometric calibration ('ubercalibration'; Padmanabhan et al. 2008).

2.1 LBG sample

The LBG sample used in this work was initially defined by Planck Collaboration XI (2013) and Anderson et al. (2015), so we closely follow their methodology with only minor modifications explained below. They selected the LBGs from the flux-limited SDSS Main galaxy sample, using the Value-Added Galaxy Catalog (VAGC; Blanton et al. 2005) `all0` sample with a constant flux limit of $r < 17.7$, including absolute magnitudes and stellar mass estimates using KCORRECT (Blanton & Roweis 2007), which fits stellar population synthesis models to the five-band photometry assuming a Chabrier (2003) stellar initial mass function (IMF). This catalogue was based on the seventh data release of the SDSS (Abazajian et al. 2009).

LBGs were selected in Planck Collaboration XI (2013) and Anderson et al. (2015) by defining cylinders of radius 1 Mpc, extending $\pm 1000\,\mathrm{km\,s^{-1}}$ in the redshift direction, and requiring that each LBG be the brightest galaxy in its cylinder according to the *r*-band absolute magnitude. In addition, a photometric redshift catalogue (Cunha et al. 2009) was used to eliminate LBG candidates with a brighter companion without a spectroscopic redshift due to fibre collisions. The only difference between these earlier works and this one is that the LBG isolation criteria were previously imposed using a *Wilkinson Microwave Anisotropy Probe* 7 (*WMAP*7) cosmology (Komatsu et al. 2011), but here we use the cosmology of Planck Collaboration XVI (2014). Imposition of these selection criteria left 279 343 LBGs, of which we use the 249 818 that lie within the area covered by the SDSS source catalogue described in Section 2.2.

Table 1. Summary of the properties of the galaxy samples included in each colour and stellar mass bin in this analysis. The quantities that are tabulated are the minimum and maximum stellar mass, the number of galaxies $N_{\rm gal}$, the effective weighted stellar mass of the galaxies taking into account their effective weight in the lensing measurement for our canonical (VAGC) stellar masses and the MPA/JHU stellar masses, the effective weighted redshift $z_{\rm eff}$ of the galaxies in the bin including the lensing weight and the fraction of Main sample galaxies $f_{\rm LBG}$ in this bin that are selected as LBGs.

$\log_{10}\left(\frac{M_{*,\rm min}}{\rm M_\odot}\right)$	$\log_{10}\left(\frac{M_{*,\rm max}}{\rm M_\odot}\right)$	$N_{\rm gal}$	$\log_{10}\left(\frac{M_{*,\rm eff}}{\rm M_\odot}\right)$	$\log_{10}\left(\frac{M^{\rm MPA}_{*,\rm eff}}{\rm M_\odot}\right)$	$z_{\rm eff}$	$f_{\rm LBG}$
			Red			
10.0	10.4	4244	10.28	10.39	0.064	0.13
10.4	10.7	17 542	10.58	10.70	0.081	0.27
10.7	11.0	44 724	10.86	10.97	0.105	0.47
11.0	11.2	37 987	11.10	11.20	0.131	0.66
11.2	11.4	28 008	11.29	11.38	0.159	0.79
11.4	11.6	12 599	11.48	11.56	0.191	0.88
11.6	15.0	3195	11.68	11.75	0.230	0.91
			Blue			
10.0	10.4	20 690	10.24	10.29	0.079	0.32
10.4	10.7	30 842	10.56	10.63	0.100	0.48
10.7	11.0	33 621	10.85	10.94	0.124	0.65
11.0	11.2	11 040	11.10	11.18	0.155	0.79
11.2	11.4	2626	11.28	11.35	0.183	0.87
11.4	11.6	325	11.47	11.54	0.220	0.90
11.6	15.0	96	11.68	11.69	0.246	0.96

We divide the galaxy sample into red and blue LBGs based on the $g-r$ colour K-corrected to $z=0.1$, using

$$^{0.1}g - ^{0.1}r = 0.8 \quad (1)$$

for our dividing line. As discussed in Zu & Mandelbaum (2015a), the adoption of a stellar mass-dependent colour cut to better isolate the red sequence modifies the fractions of galaxies in the red and blue subsamples by at most 3 per cent for the highest and lowest stellar mass subsamples, so the choice of a constant dividing line has little impact on our results. Finally, we require redshift $z \geq 0.03$, excluding the very small fraction of the sample at low redshift where the high galaxy flux at fixed luminosity induces more significant systematic uncertainty in sky subtraction and measurements of galaxy properties.

Since the interpretation of stacked lensing signals can be complicated in the cases where the mass distribution is extremely broad, we define relatively narrow bins in stellar mass. The halo mass distribution will still be broad due to intrinsic scatter between stellar and halo mass, but it improves the situation compared to that with very broad stellar mass bins. However, relatively few high stellar mass LBGs are classified as blue, so we also present results for one very broad bin of blue galaxies above a stellar mass threshold of $10^{11}\,{\rm M}_\odot$. The properties of the LBG samples in each stellar mass and colour bin are summarized in Table 1. In addition, the number of galaxies and the LBG fraction as a function of redshift z and stellar mass M_* are shown in Fig. 1. The table and figure clearly indicate the scarcity of blue LBGs at high M_*. As shown, the fraction of Main sample galaxies that are LBGs is highest at high stellar mass.

Fig. 1 illustrates that the sample is quite far from volume limited. We investigated the importance of the non-volume-limited nature of the sample by calculating LBG lensing signals for $z < 0.08$, resulting in substantial reduction in sample size for all stellar mass bins except the first two (which are still not quite volume limited after making this cut). However, while the error bars increased significantly, there is no strong modification in the lensing signal, just a slight shallowing below $100\,h^{-1}$ kpc. For a direct comparison of the lensing signals between the full LBG sample and the $z < 0.08$ subsample, see Appendix A. As discussed in Section 5.3, these differences do not systematically change mass estimates in a way that suggests that a lack of volume-limited sample is driving our results, so for the rest of this paper we proceed with the flux-limited samples described above.

Since many previous papers that have explored the relationship between stellar and halo mass used the MPA/JHU stellar mass estimates[2] [an updated version of the Kauffmann et al. (2003) catalogue] instead of those from the VAGC, Table 1 includes the effective mean stellar mass for each sample using the MPA/JHU masses (with a colour- and stellar mass-dependent conversion applied based on comparison between the catalogues). The differences are typically 0.1 dex for red galaxies, and slightly less for blue galaxies, with the correction being larger at low stellar mass. While we adopt the VAGC stellar masses as our canonical ones used for the analysis, to facilitate the comparison with previous work we will plot the results in Section 5.4 as a function of the MPA/JHU masses, denoted $M_*^{\rm (MPA)}$.

2.2 Source sample

To measure the galaxy–galaxy lensing signal, we use a catalogue (Reyes et al. 2012) of 1.2 background galaxies per arcmin^2 with galaxy shape measurements (corrected for the effects of the point spread function) estimated using the re-Gaussianization method (Hirata & Seljak 2003) and photometric redshifts from Zurich Extragalactic Bayesian Redshift Analyzer (Feldmann et al. 2006). The catalogue is characterized in detail in several papers (see Mandelbaum et al. 2012, 2013; Nakajima et al. 2012; Reyes et al. 2012), with well-understood systematic uncertainties.

3 MOCK CATALOGUES

We use one particular Munich SAM, a simulation of the development of the galaxy distribution self-consistently including evolution

[2] http://www.mpa-garching.mpg.de/SDSS/

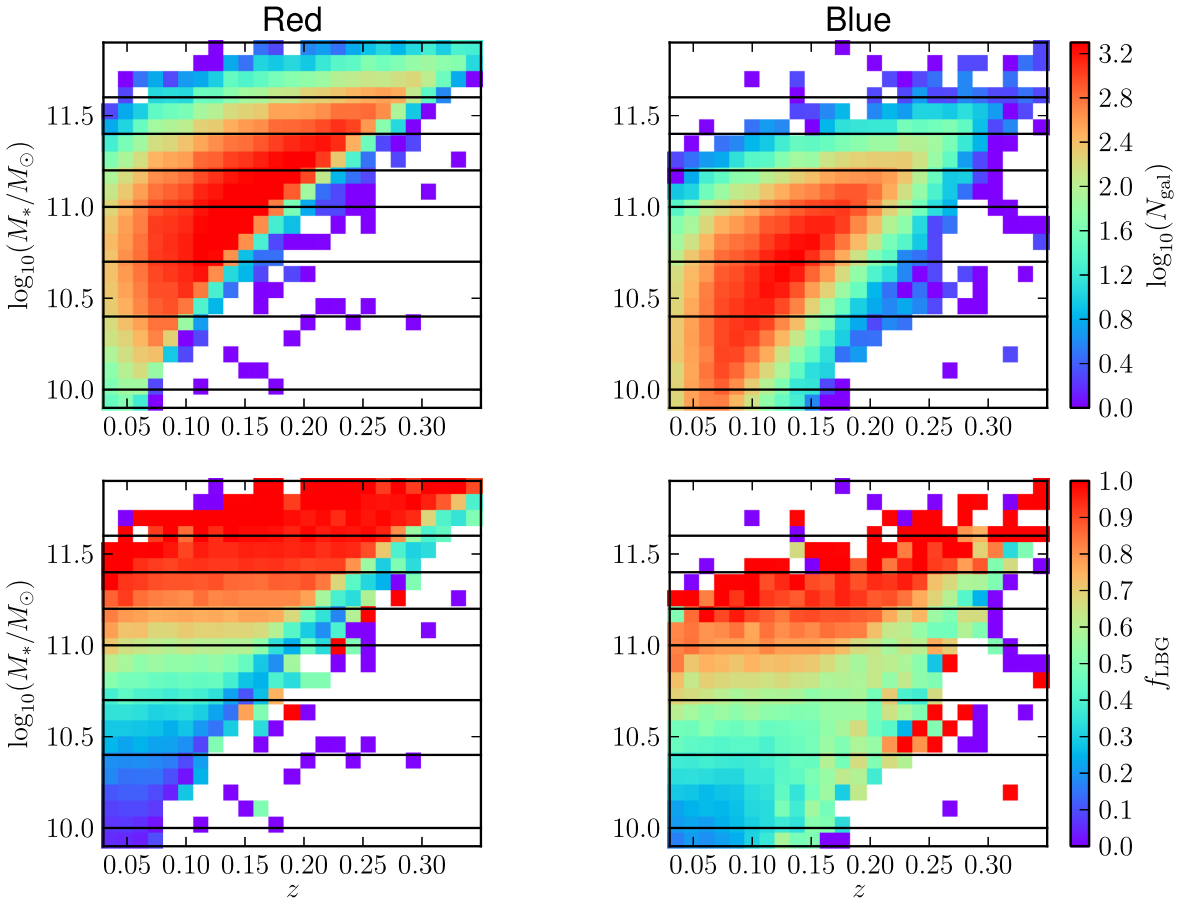

Figure 1. Top and bottom rows show the log of the number of LBGs and the fraction of Main sample galaxies that are selected as LBGs, respectively, as a function of redshift and stellar mass. Results for red and blue galaxies are shown separately in the left and right columns. The colour scales are defined self-consistently across the two columns. Horizontal lines indicate the edges of the bins in stellar mass used for our analysis.

and the gravitational environment, to create mock catalogues that are used to calibrate the mass biases and satellite contamination. The formation and evolution of galaxies are modelled following the physics in the Guo et al. (2011) model. Central galaxies are located at the centre of the friends-of-friends (FOF) haloes, while satellite galaxies are in subhaloes that are not at the centre of FOF haloes and may include orphan galaxies for which the dark matter subhalo was disrupted before the present time. The stellar mass and photometric properties of model galaxies are determined using stellar population synthesis models from Bruzual & Charlot (2003) with the Chabrier (2003) IMF. The uncertain star formation and feedback efficiencies were tuned to produce close fits to the stellar mass function of low-redshift galaxies from SDSS. We further used an abundance matching-based method to correct the stellar masses by small amounts in order to bring the model stellar mass function into exact agreement with that in the SDSS (see Wang et al. 2016 where this particular model is denoted G11-P'). The model also reproduces the observed luminosity and auto-correlation functions of galaxies (Wang et al. 2016).

The original Guo et al. (2011) model is based on the Millennium Simulation (MS; Springel et al. 2005), with *WMAP*1 ΛCDM cosmological parameters (Spergel et al. 2003). In our analysis, we scale the original MS to the first-year *Planck* cosmology (Planck Collaboration XVI 2014, $H_0 = 67.3$, $\Omega_{\rm m} = 0.315$ and $\Omega_\Lambda = 0.685$), by adopting the scaling algorithm developed by Angulo & White (2010) and improved by Angulo & Hilbert (2015). Thus, in the end, the model has the same physics and parameters as Guo et al. (2011) but is based on the *Planck* cosmology. As shown in Angulo & White (2010), the rescaling algorithm can (in most respects) accurately reconstruct the matter field and properties of dark matter haloes as they would have been simulated with another cosmological model; however, the concentrations of dark matter haloes are less well reproduced. We show the sensitivity of our results to the assumptions in the halo concentration versus mass relation in Section 5.3.

3.1 Mock LBG samples

We construct mock LBG catalogues using exactly the same selection criteria as for SDSS LBGs. We first project the simulation box along the z-axis (representing the line-of-sight direction). Each galaxy can be assigned a redshift based on its z coordinate and velocity. Selections can then be made based on the projected separation and redshift difference in the same way as in the observational data. The direct projection of the simulation box maximizes the statistical signal, but fails to incorporate observational effects such as the flux limit of the real survey, the K-corrections to obtain rest-frame magnitudes, and the incompleteness of close pairs caused by fibre collisions and the complex geometry of SDSS. Wang & White (2012) and Wang et al. (2014) have compared satellite properties based on such direct projections of the simulation box to a full light-cone mock catalogue, and they found that the direct projection gives unbiased results. For our later analysis, we will use both LBGs in the

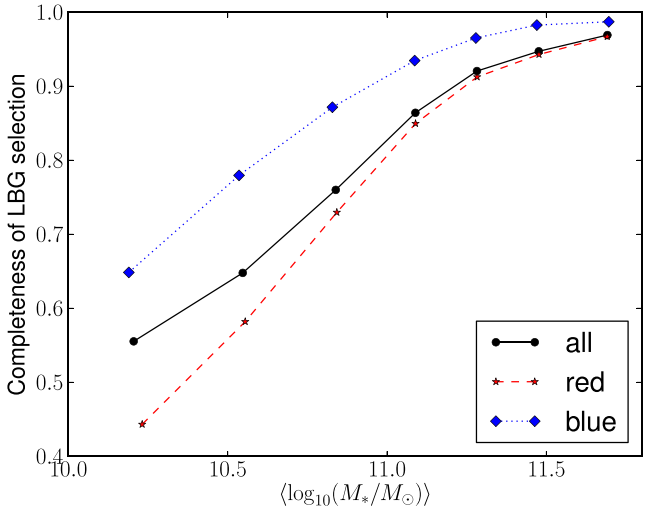

Figure 2. The completeness of the central galaxy selection as carried out using the LBG criterion in stellar mass bins, for red, blue and all LBGs shown as red, blue and black points, respectively.

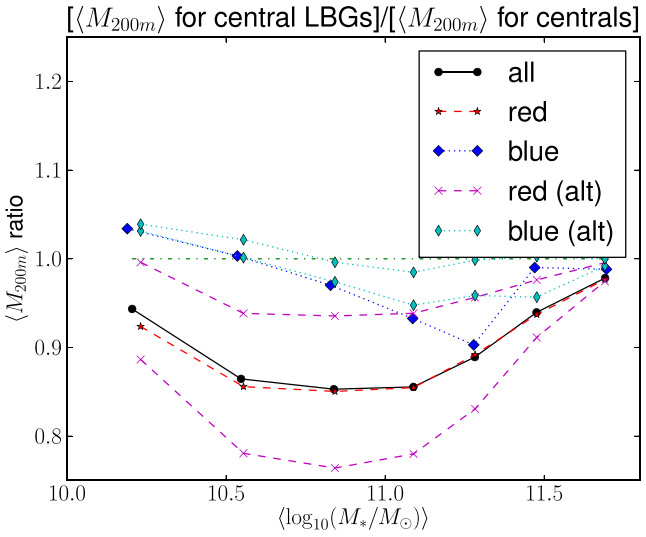

Figure 3. The ratio of the mean halo mass of central LBGs to the mean halo mass of all centrals in stellar mass bins, for red, blue and all LBGs shown as red, blue and black points, respectively. The additional magenta and cyan points labelled as 'alt' in the legend were calculated using alternate mock catalogues that will be discussed in more detail in Section 5.3, as a way of quantifying systematic uncertainty in these results.

$z = 0$ snapshot and those in earlier snapshots to account properly for the evolution of galaxies and their haloes. However, we have confirmed that the halo mass distributions as a function of stellar mass and colour do not differ very strongly between the $z = 0$ snapshot and the multi-snapshot catalogues.

To further validate our use of these mock catalogues for this study, in Section 5.1, we will compare the lensing profiles of the simulated LBG samples in stellar mass and colour subsamples with those of real LBGs. In Wang et al. (2016), the predicted dark matter profiles from eight different SAMs with varying cosmology and model physics are compared with SDSS lensing profiles, and this particular model is the one that gives the best match to SDSS. However, that comparison uses only stellar mass binning of the sample, so our test here using colour divisions may be considered a more stringent test.

3.2 Completeness and purity of central galaxy samples

3.2.1 Completeness

First, we use the $z = 0$ snapshot of the mock catalogue to assess the completeness of the sample of central galaxies selected using the LBG cut. The completeness is quantified as the fraction of central galaxies of a given stellar mass and colour that pass the LBG selection criteria. We also check whether the LBG selection is independent of the host halo mass, i.e. is the typical halo mass of central LBGs the same as the typical halo mass of central galaxies overall? Incompleteness that causes a bias in the halo mass distribution is more problematic for our purposes. For 'typical' masses, we consider a straight average, a median and $\langle M_{200m}^{2/3} \rangle^{3/2}$; since the mass from an NFW fit scales like $\Delta\Sigma^{3/2}$ on small scales (e.g. Mandelbaum et al. 2010), averaging $\Delta\Sigma$ corresponds to averaging $M_{200m}^{2/3}$. However, since most methods measure $\langle M_{200m} \rangle$, we will use that as our canonical statistic for comparison of masses throughout this work, and apply corrections to best-fitting masses to get an average halo mass.

The completeness is shown in Fig. 2, and the ratio of typical central LBG halo mass to typical central galaxy halo mass is shown in Fig. 3. As Fig. 2 illustrates, the completeness of the central galaxy sample selected using the LBG criterion is quite high (>90 per cent) for stellar masses above 10^{11} $M_\odot$, but drops below that. There are two reasons for this incompleteness. First, as discussed in Planck Collaboration XI (2013), many of the 'missing' central galaxies were excluded because they are not the brightest object in their own halo [this explanation is also qualitatively consistent with the results of Skibba et al. (2011) and Hoshino et al. (2015)]. Secondly, the typical halo masses of the central galaxies with stellar mass below 10^{11} $M_\odot$ are such that the 1 Mpc cylinder used in the LBG selection exceeds the virial radius. Hence, low stellar mass centrals can be excluded because of a brighter galaxy within a distinct neighbouring halo. This effect is more important for red than for blue LBGs, presumably since red galaxies tend to occupy more overdense regions.

However, for this study we are more concerned with the results in Fig. 3, which indicate whether the mean halo mass of central LBGs differs significantly from the mean halo mass of all centrals. The former is what we measure, but the latter is what we wish to infer. As shown, for blue galaxies the ratio of these mean halo masses always exceeds 0.9. For red galaxies, which suffer from more incompleteness, the ratio can be as low as 0.85, meaning that red central LBGs have masses that are biased low by about 15 per cent relative to those of all red centrals at the same stellar mass. The curves for 'red' and 'all' have similar trends that arise due to their having broader halo mass distributions than the 'blue' sample, so even a slight mass dependence in the LBG selection can more easily modify the mean halo mass. Moreover, the 'red' and 'all' curves are similar because the contribution of red LBGs to the 'all' curve is boosted by the overall higher halo masses for red LBGs. If the ratios in Fig. 3 had been very far from 1 (e.g. 0.5), then this would call our entire method into question; but we will correct for this bias using the curves in Fig. 3, relying on the realism of the mock catalogues to provide valid corrections.

We emphasize that Fig. 3 rules out the idea that we might observe different halo masses for the red versus blue LBG samples solely due to selection effects (e.g. that the red LBG sample might be heavily biased towards high-mass haloes due to the selection

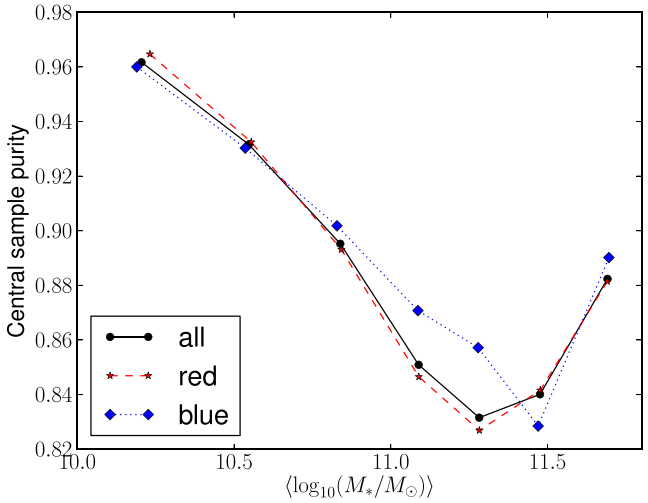

Figure 4. The purity of the central galaxy sample obtained using the LBG criterion in stellar mass bins, for red, blue and all LBGs shown as red, blue and black points, respectively.

procedure preferentially excluding low-mass red centrals that are in overdense regions). While the corrections derived from Fig. 3 are in principle dependent on the details of the mock catalogues, we confirm in Section 5.3 that even significant modifications in the mock catalogues do not lead to major changes in these corrections; alternative results for two different mock catalogues discussed in that section are shown in Fig. 3.

Our finding that there is a small bias in the mean halo mass due to LBG selection is consistent with the findings of More et al. (2009). They compare the results of an iterative, luminosity-dependent isolation criterion with a fixed aperture criterion (which is stricter than the one used here, as it requires a factor of 2 difference in luminosity between the LBG and anything else in its cylinder, instead of that it be strictly the brightest). As shown in their fig. A1, the fixed isolation criterion can give a stellar mass-dependent suppression of the mean halo mass of selected galaxies compared to that of all central galaxies at that stellar mass. While a quantitative comparison is not possible due to the different cylinder parameters and brightness requirements, our results are qualitatively in agreement with theirs.

3.2.2 Purity

In addition, it is important to understand the purity of the LBG sample as a set of central galaxies. Contamination from satellites can modify the shape and increase the amplitude of the weak lensing signal on scales above $\sim 300\,h^{-1}$ kpc (e.g. Mandelbaum et al. 2005b), affecting mass estimates. This effect is particularly important if the contaminating satellites reside in very high mass haloes. Thus, Fig. 4 shows the purity of the LBG sample in the $z = 0$ snapshot of the simulation, defined as the ratio of number of central LBGs to number of LBGs as a function of stellar mass and colour. As shown, at stellar masses below 10^{11} $M_\odot$, the purity of the central sample determined using the LBG selection exceeds $\sim$90 per cent. For higher stellar mass, it can go as low as 82 per cent. This is most likely related to the fact that (as mentioned in Section 3.2.1) the brightest galaxy in a halo is not always a central galaxy.

However, the magnitude of the impurity alone cannot be used to quantify how the contaminating satellites bias the mass estimates from fits to $\Delta\Sigma$. The bias in the masses depends on the details of the subhaloes and larger host haloes in which the contaminating satellites reside, the distribution of their separations from the centre of the host halo and other effects. For example, in the case of contamination due to the brightest galaxy not being the central, it may often be the case that the mass of the host halo is not very different from the mass one would expect if it had been a central, so the contamination in the lensing signal and mass estimates will not be very large. In the next section, we will quantify the implications of satellite contamination on mass estimates directly, by fitting the lensing signal in the mock LBG samples (including the contaminating satellites) to estimate masses, and directly determining the bias.

4 METHOD

4.1 Measurements

Galaxy–galaxy weak lensing, the coherent tangential shape distortion (or shear) of background galaxies due to the matter in foreground lens galaxies, probes the connection between the lens galaxies and matter via their cross-correlation function $\xi_{\rm gm}$. This cross-correlation can be related to the projected surface density[3] via

$$\Sigma(r_{\rm p}) = \overline{\rho} \int \left[1 + \xi_{\rm gm}\left(\sqrt{r_{\rm p}^2 + \pi^2}\right)\right] {\rm d}\pi, \tag{2}$$

where $\overline{\rho}$ is the mean matter density, $r_{\rm p}$ is the physical projected separation and π is the line-of-sight distance from the lens. The surface density is then related to the observable quantity for lensing, the surface density contrast

$$\Delta\Sigma(r_{\rm p}) = \gamma_{\rm t}(r_{\rm p})\Sigma_{\rm crit} = \overline{\Sigma}(< r_{\rm p}) - \Sigma(r_{\rm p}). \tag{3}$$

Here $\overline{\Sigma}(< r_{\rm p})$ is the average surface density within $r_{\rm p}$. The observable $\Delta\Sigma$ is the product of two factors, a tangential shear $\gamma_{\rm t}$ and a geometric factor

$$\Sigma_{\rm crit} = \frac{c^2}{4\pi G}\frac{D_{\rm S}}{D_{\rm L} D_{\rm LS}}, \tag{4}$$

where $D_{\rm L}$ and $D_{\rm S}$ are angular diameter distances to the lens and source, $D_{\rm LS}$ is the angular diameter distance between the lens and source, and physical (rather than comoving) coordinates are used for all quantities throughout this paper.

The lensing measurement begins with identification of lens–source pairs, with source photometric redshift larger than the lens spectroscopic redshift. Inverse variance weights are assigned to each lens–source pair, including both shape noise and measurement error terms in the variance:

$$w_{\rm ls} = \frac{1}{\Sigma_{\rm crit}^2(\sigma_{\rm e}^2 + \sigma_{\rm SN}^2)}, \tag{5}$$

where $\sigma_{\rm e}^2$ is the shape measurement error due to pixel noise and $\sigma_{\rm SN}^2$ is the root-mean-square intrinsic ellipticity [both quantities are per component, rather than total; the latter is fixed to 0.365 following Reyes et al. (2012)]. Use of photometric redshifts which have non-zero bias and significant scatter results in a bias in $\Delta\Sigma$ that can be easily corrected using the method from Nakajima et al. (2012). This bias is a function of lens redshift, and is calculated including all weight factors for each lens sample taking into account its redshift distribution.

[3] Here we neglect the very broad radial window function, given that it makes sub-0.2 per cent differences in the signals on the scales used in this work, and neglecting it enables faster computations of theoretical signals.

$\Delta\Sigma$ in bins in $r_{\rm p}$ can be computed via a summation over lens–source pairs 'ls' and random lens–source pairs 'rs':

$$\Delta\Sigma(r_{\rm p}) = \frac{\sum_{\rm ls} w_{\rm ls} e_{\rm t}^{\rm (ls)} \Sigma_{\rm crit}(z_{\rm l}, z_{\rm s})}{2\mathcal{R} \sum_{\rm rs} w_{\rm rs}}, \quad (6)$$

where $e_{\rm t}$ is the tangential ellipticity component of source galaxy with respect to the lens position, and $\mathcal{R}$ is the shear responsivity (Bernstein & Jarvis 2002) that converts from the ensemble average distortion to shear. The division by $\sum w_{\rm rs}$ accounts for the fact that some of our 'sources' are physically associated with the lens, and therefore not lensed by it (see, e.g., Mandelbaum et al. 2005a). Finally, we subtract off a similar signal measured around random points with the same area coverage and redshift distribution as the lenses, to subtract off any coherent systematic shear contributions (Mandelbaum et al. 2005a); this signal is statistically consistent with zero for all scales used in this work.

To calculate the error bars on $\Delta\Sigma$, we use the bootstrap resampling method, dividing the lens sample into 100 patches on the sky. Previous work (e.g. Mandelbaum et al. 2005a, 2013) has shown that for the scales used here, the error bars are dominated by uncorrelated shape noise (whereas on larger scales, correlated shape noise, systematics and cosmic variance result in non-negligible correlations between bins in $r_{\rm p}$). For this reason, we use only diagonal errors throughout this work. The maximum scale used for the fits in the lensing analysis is 1 h^{-1} Mpc, which for a typical lens redshift is far below the typical size of each jackknife resampled region. Thus, the bootstrap method is a reasonable approach to getting the covariance matrix for the projected mass profile, and has been shown to agree with several other approaches in the shape noise-limited regime (Mandelbaum et al. 2005a).

4.2 Mass estimation

When estimating masses, we take advantage of the simplicity of the LBG sample as a nearly pure sample of central galaxies. All of the projected mass around these lens galaxies contributes to the galaxy–galaxy lensing signal. This includes contributions from the host dark matter halo in which the lens galaxy resides ('one-halo term'), and from other dark matter haloes ('two-halo term') that are part of large-scale structure associated with the lens. For central galaxies, the one-halo term simply corresponds to the $\Delta\Sigma$ for the host dark matter halo. For satellite galaxies, there are two contributions to the one-halo term: on small scales, a contribution from the satellite subhalo, and on larger scales (0.3–2 h^{-1} Mpc) a contribution from the host halo itself. For a nearly pure sample of central galaxies, we can restrict ourselves to the one-halo regime and take advantage of the fact that the halo profiles of centrals are approximately NFW (Navarro, Frenk & White 1997) profiles.

For all but the highest mass bin, we use a minimum radius of $r_{\rm p} = 50\,h^{-1}$ kpc (physical), whereas for the highest mass bin where there is evidence of large-scale light profiles interfering with the measurements of the nearby fainter galaxies used for lensing measurements, our minimum scale is $r_{\rm p} = 70\,h^{-1}$ kpc. The contribution of the galaxy stellar mass to the lensing signal is negligible compared to the dark matter halo contribution for $r_{\rm p}$ above our minimum value. In all cases, the maximum scale is 1 h^{-1} Mpc, ranging from several times the virial radius to only a small amount outside the virial radius. We rely on the calibration factors derived from using the same fitting procedure on mock catalogues to correct for any small contamination of the signal on these scales by the two-halo term, which may be more important at lower mass (where we go farther beyond the virial radius).

Our fits have a fixed concentration–mass relation, corresponding to that from Diemer & Kravtsov (2015), and evaluated at the lensing-weighted mean redshift of each sample. However, when presenting our results we will estimate the sensitivity of our results to assumptions about the concentration–mass relation. The masses quoted in this paper correspond to a spherical overdensity of 200 with respect to the mean density (M_{200m}), using Planck Collaboration XVI (2014) cosmological parameters ($\Omega_{\rm m} = 0.315$).

As shown in Mandelbaum et al. (2005b), using fits to NFW profiles when the signal is actually the average of many NFW profiles spanning a range of masses and concentrations can give a best-fitting mass that is biased with respect to the true mean mass by a few to tens of per cent (depending on the width of the mass distribution). This point is quite relevant given that Planck Collaboration XI (2013) showed that the typical full width at half-maximum of the halo mass distribution at fixed stellar mass for LBGs is $\sim$1 dex. In addition, NFW fitting can result in mass biases if the assumed concentration is incorrect, or if the fit includes scales outside the virial radius where the simple extrapolation of the NFW profile may be incorrect. Our approach in this work is to use *N*-body and SAM-based mock catalogues to calibrate out such biases as well as those due to satellite contamination in our LBG sample (see Section 3).

Error bars on the mass estimates are calculated using the bootstrap. Each bootstrap-resampled $\Delta\Sigma$ is fitted using the procedure described in this section, and the quoted results are the median of the mass distribution from all bootstrap-resampled data sets, with error bars indicating the 16 and 84 percentiles. For all but the lowest mass bin (for red and blue) and the two highest mass blue samples, where the signal-to-noise (S/N) is lower, using these percentiles gives nearly identical errors to using the standard deviation. Also, the median of the bootstrap masses is consistent with the mass obtained by directly fitting the average signal to within $\lesssim 0.1\sigma$. It should be kept in mind that we are quoting percentiles of the distribution of mean halo mass values from the bootstrap; these are errors on the mean mass, not a measure of scatter in the halo mass distribution (which is much broader than our quoted errors on the mean).

To summarize, we are inferring $\langle M_{200m}\rangle(M_*)$, the average halo mass in bins of stellar mass. This is the most observationally accessible quantity in a lensing measurement. Other works describe the relationship between stellar and halo mass in other ways. For example, halo models commonly infer a stellar-to-halo mass relation (SHMR) parametrized as $M_*(M_{200m})$ which is a continuous function representing the median stellar mass of central galaxies occupying haloes of fixed halo mass. In principle, the quantity that we measure in this work for red and blue central galaxies depends on all of the following: the continuous SHMR, the size of the intrinsic and observational scatter about the median SHMR, the halo mass function, and any halo mass dependence in the fraction of red versus blue galaxies. It is important to bear in mind the distinction between the observationally accessible $\langle M_{200m}\rangle(M_*)$ and the underlying SHMR when comparing our results with others that infer a parametrized $M_*(M_{200m})$.

4.3 Fidelity of mass estimation procedure

Next, we consider the fidelity of the mass estimates from our NFW fitting procedure. The average of a collection of NFW profiles does not look precisely like an NFW profile with the average mass, and simplifications in the assumed mass–concentration relation along with deviations from an NFW profile extrapolated beyond the virial

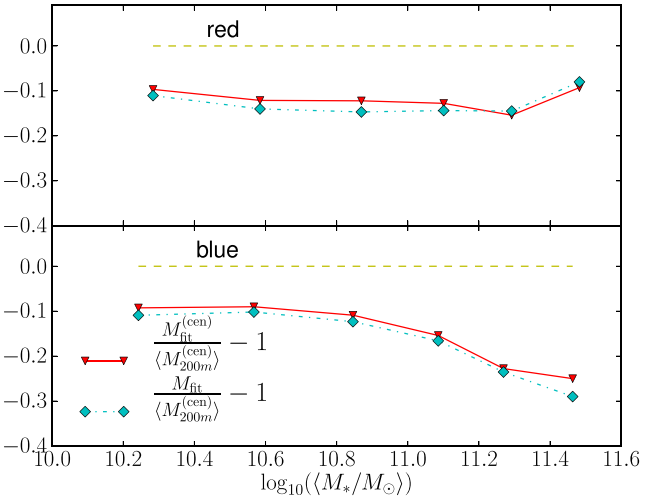

Figure 5. The bias in the best-fitting NFW mass compared to the mean halo mass for central LBGs, for red (top) and blue (bottom) LBGs, respectively. The two lines that are shown indicate the bias in the estimated masses of central LBGs, which result from the fitting procedure, and in the estimated masses of all LBGs (including those that are not central, thus including the effects of satellite contamination). The ideal unbiased case is shown as a horizontal dashed line.

radius can cause biases. To quantify these effects, we applied our mass fitting procedure to stacked $\Delta\Sigma$ profiles for *central* LBGs selected across multiple redshift snapshots in the mock catalogues.

A second complication is that satellites that are accidentally included in the LBG sample, which are not completely negligible (Section 3.2.2), modify the $\Delta\Sigma$ profiles on intermediate scales and bias the mass estimates. To address this point, we applied our mass fitting procedure to stacked $\Delta\Sigma$ profiles for *all* (not just central) LBGs selected across multiple redshift snapshots while matching the joint redshift–stellar mass distribution of the real LBG sample, and including redshift-dependent weights consistent with the lensing analysis in the real data as in Wang et al. (2016). This test also includes the issues covered by the first test, but carrying out both tests separately allows us to assess the relative importance of satellite contamination versus other issues.

Results are shown in Fig. 5, where we plot the bias of the best-fitting masses with respect to the true average halo mass for central galaxies in this stellar mass bin, defined as the ratio of the best-fitting mass to the average central galaxy halo mass, minus 1. For the overall LBG sample, this is denoted $M_{\rm fit}/\langle M_{200m}^{\rm (cen)}\rangle - 1$, while for central LBGs it is denoted $M_{\rm fit}^{\rm (cen)}/\langle M_{200m}^{\rm (cen)}\rangle - 1$. As shown, the bias tends to be negative, i.e. an underestimation of the mean mass. This is also true if we use the lensing signal-weighted average mass ($\langle M_{200m}^{2/3}\rangle^{3/2}$), which makes the bias slightly less severe. Our finding that the best-fitting mass is below the mean mass is consistent with the results of Mandelbaum et al. (2005b), who found that when assuming a single value of mass, the best-fitting mass tended to be below the mean mass and above the median mass. In that work, the bias was worse when the mass distribution was broader. Fig. 6 shows that this is the case here too, though the trend with breadth of the halo mass distribution is weak; the bins in Fig. 5 that have a larger bias for blue LBGs at high stellar mass have a broader halo mass distribution, also resulting in a bigger difference between $\langle M_{200m}\rangle$ and $\langle M_{200m}^{2/3}\rangle^{3/2}$.

The difference between the results for the two tests shown in Fig. 5 is very small, indicating that satellite contamination is not significantly biasing the mass fits, perhaps for the reasons suggested

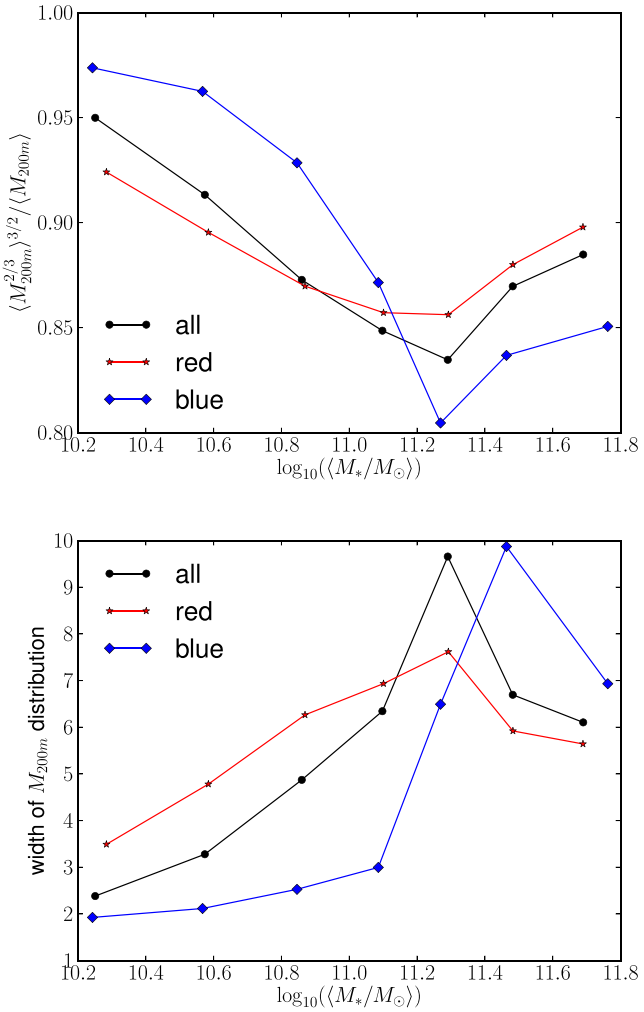

Figure 6. Top: the ratio of the lensing signal-weighted average mass ($\langle M_{200m}^{2/3}\rangle^{3/2}$) to the mean mass $\langle M_{200m}\rangle$ for central LBGs in the mock catalogue. Bottom: the width of the halo mass distribution, quantified as the ratio of the halo masses corresponding to the 84th and 16th percentile of the central LBG halo mass distribution.

in Section 3.2.2. Moreover, the biases in the masses for red and blue galaxies are fairly similar, so they should not compromise our ability to distinguish between the haloes of red and blue galaxies.

5 RESULTS

5.1 Lensing signals

Fig. 7 shows the lensing signals for the LBGs in stellar mass bins, for red and blue LBGs.[4] We first consider the basic question of consistency between the signals for red and blue galaxies for $50 \leq R \leq 1000\ h^{-1}$ kpc. We carry out a non-parametric χ^2 test for consistency, defining

$$\chi^2 = \sum_i \frac{(\Delta\Sigma_{\rm red} - \Delta\Sigma_{\rm blue})^2}{\sigma^2_{\Delta\Sigma_{\rm red}} + \sigma^2_{\Delta\Sigma_{\rm blue}}}, \quad (7)$$

[4] The data shown in Figs 7–9 can be downloaded in machine-readable format from https://github.com/rmandelb/mandelbaum-data.

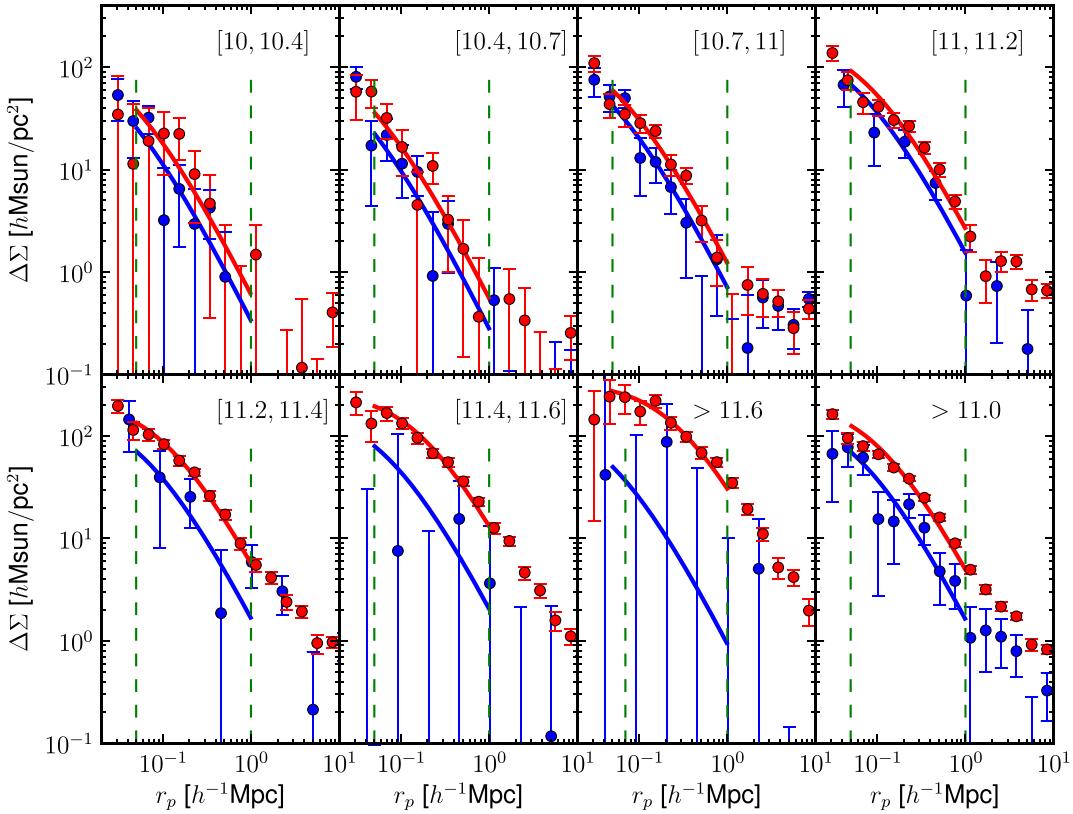

Figure 7. Lensing signals for LBGs in stellar mass bins, for red and blue LBGs shown as red and blue points with errors, respectively. The thick lines show the best-fitting NFW profiles, while the vertical dashed lines show the lower and upper limits in r_p used for the fits. For viewing purposes, the data for blue LBGs in the four narrow bins with $M_* > 10^{11}\,M_\odot$ have been rebinned into bins that are twice as broad as those shown for red LBGs, due to the lower S/N ratio.

Table 2. Results of a χ^2 test for consistency between the lensing signal for red and blue LBGs in each stellar mass bin, and across all stellar masses. This test uses the signals from 50 to 1000 h^{-1} kpc.

Stellar mass range	d.o.f.	χ^2	p-value
[10, 10.4]	15	19.7	0.18
[10.4, 10.7]	15	18.8	0.22
[10.7, 11]	15	26.8	0.03
[11, 11.2]	15	24.2	0.06
[11.2, 11.4]	15	29.8	0.01
[11.4, 11.6]	15	28.7	0.02
>11.6	15	18.8	0.22
All	105	166.9	1.2×10^{-4}

where the summation is carried out over bins in r_p. This test is interesting when the stellar mass distributions for red and blue LBGs within the bin are sufficiently similar that differences in $\Delta\Sigma$ cannot come just from the different stellar mass distributions (this condition is violated by the broad $M_* > 10^{11}\,M_\odot$ bin, which is excluded from this test).

Table 2 shows the χ^2, degrees of freedom and p-values for each stellar mass bin and combined across all stellar mass bins. The number of degrees of freedom appears larger than expected from the number of data points in Fig. 7 because the data were rebinned in the figure to make it easier to read. As shown, adopting the convention that $p < 0.05$ indicates a lack of consistency between the red and blue samples, there is a clear inconsistency for three of the bins, and a marginal inconsistency ($p = 0.06$) for a fourth bin. In the other bins, the error bars are sufficiently large for the blue LBG sample that it is difficult to draw any conclusion. The χ^2 over all seven bins is $p = 1.2 \times 10^{-4}$, ruling out the null hypothesis that red and blue galaxies at all stellar masses in this work have consistent distributions of halo masses.

As another diagnostic of the lensing profiles, we also consider the lensing profiles of all SDSS Main sample galaxies using the same stellar mass and colour divisions, but without the LBG selection imposed. This provides an alternative means (besides the mock catalogues used in Section 3) of checking whether the LBG selection chooses a biased subset of the central galaxies. Ideally, the characteristic 'bump' that satellites can cause on ∼300–1 h^{-1} Mpc scales should disappear when comparing the signal for all Main sample galaxies against that for LBGs, but the signal on smaller scales should be essentially preserved. This comparison is shown in Figs 8 and 9 for blue and red LBGs, respectively. Fig. 8 uses a single wide bin at high stellar mass due to the small number of blue galaxies above $M_* > 10^{11}\,M_\odot$. As shown, the signals for blue Main sample galaxies and LBGs in a given stellar mass bin are nearly identical, with the LBGs showing some signal deficits above ∼300 h^{-1} kpc as expected. The differences are small presumably because only a small fraction of blue galaxies tend to be satellites in higher mass haloes (e.g. Mandelbaum et al. 2006). For the red galaxies, as shown in Fig. 9, the signals for Main sample red galaxies and LBGs at fixed stellar mass are quite consistent below ∼300 h^{-1} kpc, and show a characteristic difference above that indicating that many Main sample red galaxies are satellites (especially at lower stellar mass), and that the LBG selection is effectively removing most or all of

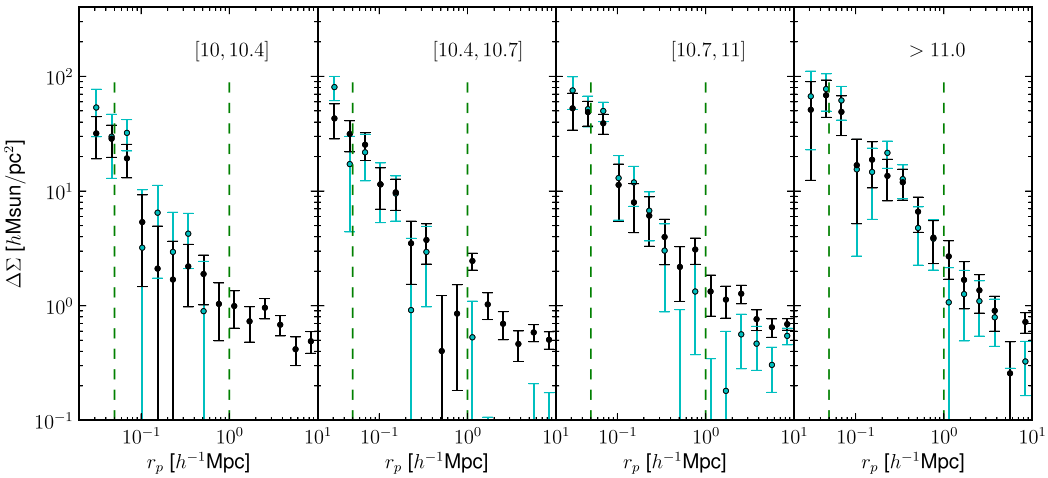

Figure 8. Lensing signals for blue Main sample galaxies versus blue LBGs in stellar mass bins shown as black and light blue points with errors, respectively. The vertical dashed lines show the lower and upper limits in r_p used for the fits of the LBG signals to NFW profiles.

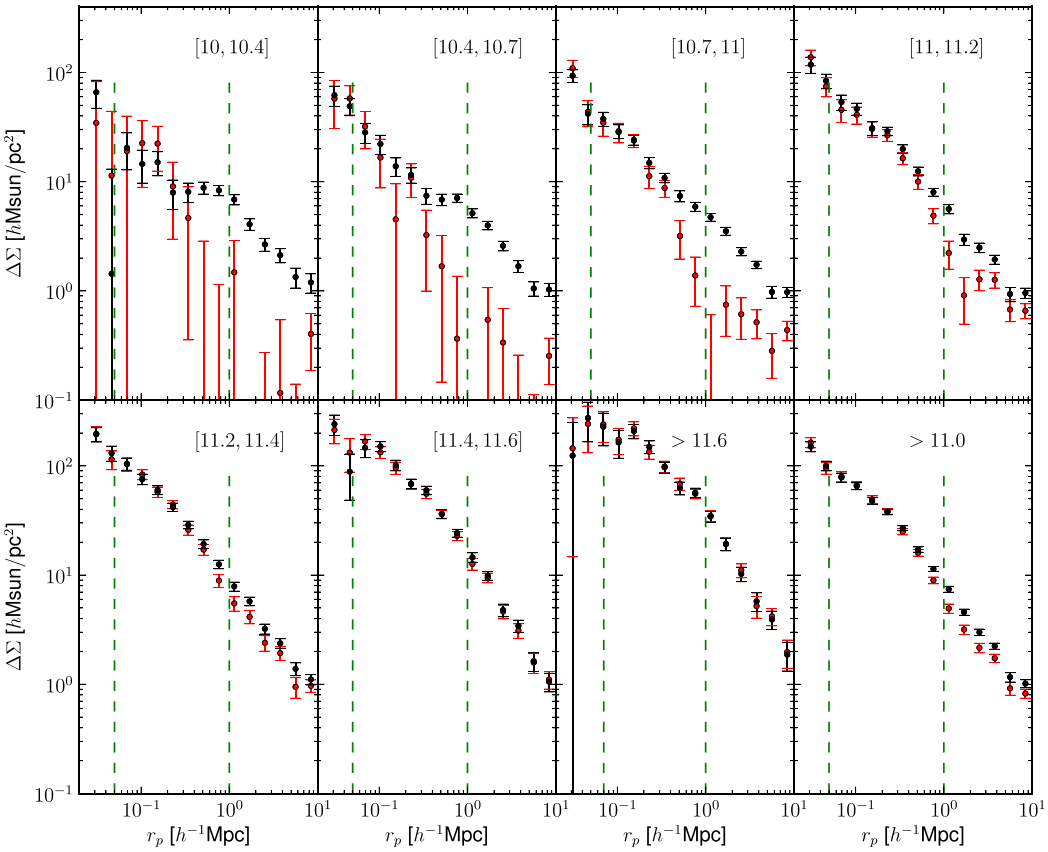

Figure 9. Lensing signals for red Main sample galaxies versus red LBGs in stellar mass bins shown as black and red points with errors, respectively. The vertical dashed lines show the lower and upper limits in r_p used for the fits of the LBG signals to NFW profiles.

the satellites. This result provides a separate validation of the LBG criterion as a way of selecting a fair sample of central galaxies, in addition to the mock catalogue-based validation from Section 3.

Finally, as a validation of our use of mock catalogues to correct for biases in the fitting procedure, Fig. 10 shows, for all stellar mass bins and both colours, a comparison between the real LBG $\Delta\Sigma$ and the LBG $\Delta\Sigma$ profiles in the mock catalogues. These were computed via direct cross-correlation of the simulated LBGs and the (subsampled) dark matter density distribution in the simulations. It is important to keep in mind that these are not fits, and that the SAM in the mock catalogues was not specifically tuned to fit lensing profiles at all. With that caveat in mind, the agreement between the data and mock catalogues is quite remarkable especially for the bins with $M_* < 10^{11.2}\,\mathrm{M}_\odot$. While the signal for blue galaxies in the mocks is slightly high compared to that in the data, the match is in general close enough that the mocks cannot have too different a halo mass distribution (as a function of stellar mass and colour) compared to the real data; for a more detailed exploration of this point, see

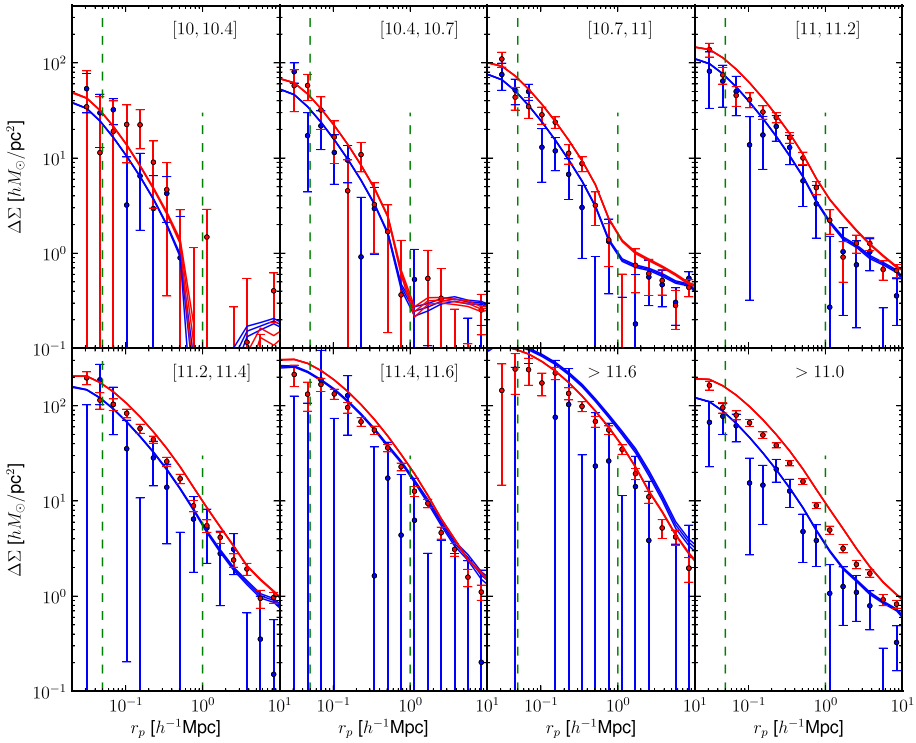

Figure 10. For all stellar mass bins as labelled on the plot, we compare the lensing $\Delta\Sigma$ profiles for red and blue LBGs in the data (the points with errors, same as in Fig. 7) with those in the mock catalogues (the solid lines). The vertical dashed lines show the lower and upper limits in r_p used for the fits of the LBG signals to NFW profiles.

Wang et al. (2016). The possible exception to this statement is in the bins with $M_* > 10^{11.4}\,\mathrm{M}_\odot$, in which there are almost no lenses in the real data, and our constraints are therefore extremely weak. The red LBG data in the highest mass bins show more tension, at roughly the 20 per cent level (30 per cent in mass).

5.2 Mass estimates

In this section, we present mass estimates for the red and blue LBG samples. Results are shown in Fig. 11. For the two lowest mass samples, the mass difference (red − blue) is consistent with 0 at approximately the 1.5σ level, while for the higher stellar mass samples, the difference is positive at $>2\sigma$.

The results in Fig. 11 include the corrections from mock catalogues necessary to ensure unbiased recovery of the average central halo masses, described in Section 3. In particular, we include two separate corrections: a colour- and stellar mass-dependent correction for biases in the fitting procedure in recovering $\langle M_{200m}\rangle$ (due to basic inadequacy of the NFW fitting, plus satellite contamination; Section 4.3), and a correction for the fact that the central LBG sample has a slightly different average mass compared to the full central galaxy sample (Section 3.2). As shown previously, these corrections go in the same direction for red and blue galaxies, with slightly different magnitude. The top panel of Fig. 11 also shows the results without the corrections; it is clear that these corrections cause $>1\sigma$ changes in the mass estimates, but are not the reason for our conclusion that red and blue central galaxies have different average halo masses in fixed stellar mass bins.

The corrected values of mass and their uncertainties are tabulated in Table B1 of Appendix B.

5.3 Systematic error budget

Here we discuss the primary sources of systematic uncertainty in our results. As discussed in Mandelbaum et al. (2013), a reasonable estimate of the multiplicative calibration uncertainty in the lensing signal using this catalogue is at most[5] 5 per cent, when considering shear systematics and photometric redshift systematics together. Since NFW mass fits scale like $\Delta\Sigma^{3/2}$ on small scales, this implies an 8 per cent overall mass calibration uncertainty at the 2σ level, correlated between all the samples (i.e. it would cause coherent shifts of all results in the same way).

However, Fig. 11 clearly reveals a more important source of systematic uncertainty. As shown, the correction factor that we apply to remove the effects of incompleteness, impurity, scatter in the mass distribution and other uncertainties in our modelling procedure is significantly larger than the statistical error for nearly all the red samples, and corresponds to roughly 1σ statistical errors for most of the blue samples. Thus, the validity of this correction factor, which encodes our understanding of multiple different issues as outlined in Section 3, is our primary source of systematic uncertainty. As already noted in Section 5.1, there are several empirical tests of the lensing signal that validate our conclusions from the mock catalogues, so we have reason to believe the uncertainty is significantly smaller than the size of the correction itself.

The corrections that were determined in Section 3 are a combination of the mass incompleteness correction and a correction to our best-fitting masses to estimate the mean mass (given the halo mass distribution, which if broad can result in significant differences between best-fitting and mean masses). The results in

[5] This should be considered more like a 2σ range than a 1σ range.

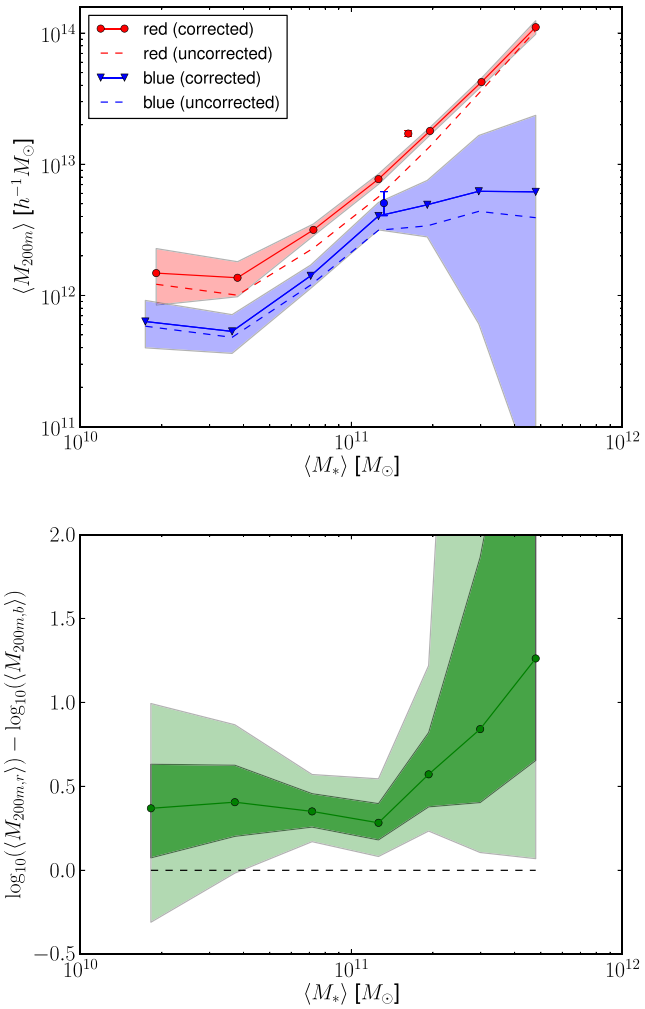

Figure 11. Top: the mean halo masses inferred from NFW fits to $\Delta\Sigma$ as a function of the average stellar mass for each bin, shown separately for red (red circles) and blue (blue triangles) LBGs, along with shaded regions showing the 16–84 percentile range. The dashed lines show results without the mock catalogue-based corrections. The single red and blue points shown separately with error bars are the results for the single bin with $M_* > 10^{11}\,\mathrm{M}_\odot$, which has a very broad stellar mass distribution that is different for the two colour samples. Bottom: the difference in mass between the red and blue samples, expressed as $\log_{10}\langle M_{200m,\,\mathrm{red}}\rangle - \log_{10}\langle M_{200m,\,\mathrm{blue}}\rangle$. The dark and light shaded regions show the 16–84 percentile and 2.5–97.5 percentile ranges, respectively.

Wang et al. (2016) provide some insight into the uncertainty in the second part of the correction factors. In that work, multiple different mock catalogues were used to model the LBG lensing and clustering signals (using the same stellar mass bins, but without colour division). The halo mass distributions were shifted by an overall multiplicative factor to match the lensing signals for LBGs in stellar mass bins, and the mean masses for all models (after this shift) were compared to get a scatter on the mean. This scatter in the mean mass reflects the different shapes of the halo mass distributions in the different models. For the seven stellar mass bins, excluding the broad one with $M_* > 10^{11}\,\mathrm{M}_\odot$, the scatters in the base-10 logarithm of the mean halo masses across all the mock catalogues are 0.035, 0.028, 0.069, 0.055, 0.060, 0.081 and 0.11 after correcting to our adopted halo mass definition. Adopting these as systematic uncertainties is somewhat conservative, given that the extreme cases that drive the scatter to large values had halo mass distributions that may have resulted in an initial failure to reproduce LBG lensing signals.

Table B1 shows that if we assume the same uncertainties for both colours, the ratios of (conservative) systematic to statistical uncertainty for red central LBGs $\langle M_{200m}\rangle$ in our stellar mass bins are 0.2, 0.2, 1.8, 1.4, 2, 2.8 and 2. For blue central LBGs, these ratios (using the smaller upper error bar) are 0.2, 0.2, 0.8, 0.6, 0.4, 0.2 and 0.2. Thus, we conclude that our conservatively adopted systematic uncertainty is subdominant to statistical errors in all cases for the blue LBGs, while for the red ones, they are comparable to the statistical errors above $M_* > 10^{10.7}\,\mathrm{M}_\odot$. However, even in the highly unlikely case that the results shift by the entirety of that systematic uncertainty in opposite directions for red and blue galaxies, this would not remove the majority of the observed mass difference between red and blue central galaxies.

To assess the systematic uncertainty in the incompleteness corrections, which account for the fact that the mean halo masses of central LBGs differ from those of all central galaxies, our procedure is as follows. We adopted two other SAMs from Guo et al. (2011) and Henriques et al. (2015), which are based on the *WMAP*1 (Spergel et al. 2003) and *Planck* (Planck Collaboration XVI 2014) cosmologies, respectively. The former has a similar semi-analytic prescription as the mock catalogue used throughout this work, whereas the latter follows a different prescription (for more detailed comparison between the LBG samples in these mock catalogues, see Wang et al. 2016). These models were specifically chosen due to the fact that their halo mass distributions at fixed stellar mass are notably different from those in our fiducial mock catalogue, resulting in a substantial mismatch when compared with the observed lensing signals (unlike for our fiducial mock catalogue), and providing a quite conservative upper bound on systematic uncertainty in the incompleteness correction. For these models, the completeness correction for blue (red) LBGs ranged from 1 to 4 per cent lower (5 per cent lower to 8 per cent higher) than our fiducial one, with some stellar mass dependence in both cases. Fig. 3 includes results from these alternate mock catalogues, in addition to our fiducial one.

As discussed in Section 2.1, the samples we use for our analysis are not volume limited. We carried out our NFW fitting procedure to signals calculated using only $z < 0.08$ LBGs to quantitatively check what happens to the best-fitting masses. We found that with the blue $z < 0.08$ LBG sample, there was a slight tendency for the NFW masses to decrease by 15 per cent compared to our main results, while for the red $z < 0.08$ LBG sample, the masses increase by typically 15 per cent. Thus, use of a volume-limited sample is not driving our conclusions about mass differences; indeed, with a $z < 0.08$ sample we would have found 30 per cent *larger* mass differences, albeit with substantially larger statistical errors as well.

Another source of systematic uncertainty is the assumed cosmology, which largely affects the values of concentration used in the fitting. We will consider this problem under the more general umbrella of concentration-related uncertainties, which also include any errors in the adopted $c(M)$ (even for the correct cosmology) and the impact of assembly bias (which could cause opposing errors in the concentrations for blue and red galaxies: red ones should reside in older haloes which are more concentrated). In principle, some errors in the $c(M)$ relation will be removed by the mock catalogue-based correction factors. For example, if the $c(M)$ relation used for the fits is wrong compared to both reality and the mocks, then our final results will be unaffected after applying the mock catalogue-based corrections. Since our primary conclusion is that red and blue central galaxies reside in haloes with different masses on average,

we focus particularly on the following question: could the impact of assembly bias on the concentrations of haloes hosting red and blue central galaxies be causing us to incorrectly draw our primary conclusion, rather than it being a real effect?

If red galaxies actually live in haloes with higher concentrations than we assumed and than in the simulations, and vice versa for blue galaxies, then the inferred halo masses for red (blue) galaxies are too high (low). The sign of this effect is therefore correct to explain our result, but it is unclear whether the magnitude could be as large as the observed halo mass differences (factors of 2–2.5). To address this question, we note that Wechsler et al. (2002) found a scatter in $\log_{10}c$ of $\sim$0.12. Taking the extreme assumption that red and blue central galaxies at fixed halo mass represent halo samples split into the upper and lower part of the $c(M)$ distribution depending on the red galaxy fraction, $\langle c_{\rm red}\rangle$ and $\langle c_{\rm blue}\rangle$ can differ by up to $\sim$35 per cent (depending on the mass range and red fraction, considering reasonable values of both quantities). Redoing the fits with modifications in concentration that are of that order for the stellar mass bin within $10^{10.7} \leq M_*/{\rm M}_\odot < 10^{11}$ causes the mass ratio to change by about 12 per cent. Even with extreme assumptions, therefore, assembly bias cannot be responsible for any sizeable part of the observed factor of 2–2.5 difference in mass between red and blue galaxies.[6] Under less extreme assumptions, there may be mass uncertainties at the few per cent level due to assembly bias affecting the halo concentrations for red and blue central galaxies. This is subdominant to the overall modelling uncertainties discussed above.

As a final test of concentration-related uncertainties, we reran the fits with the concentration free but with a lognormal prior about the adopted $c(M)$ relation used for the rest of this work. In general, the concentrations went down, and the masses went up. For red LBGs, we find that the masses typically increase by $\sim$20 per cent in the data and $\sim$11 per cent in the mocks. Thus, when we consider the change in the mass correction factor that is based on the fits to the mock catalogues, our estimated red central galaxy halo masses would go up by typically $\sim$9 per cent (but are also more noisy due to the extra degree of freedom). For blue LBGs, we find that the masses typically increase by $\sim$30 per cent in the data and $\sim$20 per cent in the mocks. Thus, the net increase in the estimated blue central galaxy halo masses when taking into account the changed correction factor would be $\sim$10 per cent. Thus, our estimates for both blue and red central halo masses would increase by $\sim$10 per cent, leaving the mass ratio unchanged on average, but noisier. The increase in noise and the lack of change in our conclusion about halo mass bimodality justify our choice to keep the fixed-concentration results as our primary ones.

5.4 Comparison with previous results

In this section, we compare our results with previous estimates of the galaxy type-dependent relationship between stellar and halo mass of central galaxies. In all cases when comparing with papers that have multiple redshift ranges, we use the closest available range. Stellar masses have been converted to our adopted units and value of h and IMF, while halo masses have been converted to our adopted convention, M_{200m} with our value of $\Omega_{\rm m}$. We have not accounted for more subtle differences in halo versus stellar mass relations that could arise from, e.g., different assumptions about halo concentration versus mass relations. Differences in stellar mass modelling can lead to additional (non-IMF-related) systematic offsets between stellar mass estimates that can be significant (Leauthaud et al. 2012b), but are difficult to estimate and correct. When comparing with previous SDSS results, we use the MPA/JHU stellar mass estimates that were adopted by many of those works. The exception to this is More et al. (2011), who used stellar masses from the Bell & de Jong (2001) approach; however, the fitting formulae in Li & White (2009) show that for the range of stellar masses used in this work, the MPA/JHU and Bell & de Jong (2001) agree on average, so we do not apply a correction. In all cases, the plotted quantity is $\langle M_{200m}\rangle$ at fixed stellar mass, either in bins in stellar mass (shown using points) or from a parametric model or continuous function based on finely binned haloes in simulations (shown using curves). The error bars indicate error on the mean, rather than intrinsic scatter about the mean.

A number of previous works measured the colour-dependent average halo mass for central galaxies in bins in stellar mass. Mandelbaum et al. (2006), Velander et al. (2014) and Hudson et al. (2015) measured galaxy–galaxy lensing by galaxies split into passive and active categories as a function of stellar mass, and used a simplified halo model to interpret the results in terms of typical central halo masses (along with a satellite term). The top-left panel of Fig. 12 shows a comparison between our results (shown as shaded regions that are the same as those in Fig. 11) and those three works. As shown, the results of Mandelbaum et al. (2006) are largely consistent with ours, with a hint of slightly lower masses for red galaxies below $M_*^{\rm (MPA)} = 10^{11}\,{\rm M}_\odot$. However, this could be a consequence of modelling differences (since a simple halo model was used to separate out satellite and central contributions, which are quite important for low-mass red galaxies). Alternatively, this is the only work against which we compare that used a morphological- rather than colour-based separator (indicated in the plot using 'early/late' instead of 'red/blue'); while morphology and colour are correlated, they do not split up the data in exactly the same way and could drive some of the observed differences. Also note that our current results have a slightly higher S/N than the earlier Mandelbaum et al. (2006) results, due to the larger area used and the better photometric redshifts for the source galaxies (which make our weighting closer to optimal). This S/N difference, combined with the slight shift for the early-type galaxies, is the reason that we now see a more statistically significant difference between the average halo masses for red and blue central galaxies even below $M_* = 10^{11}\,{\rm M}_\odot$. The Velander et al. (2014) results seem consistent with ours for red galaxies, but somewhat high for blue galaxies. The Hudson et al. (2015) results are slightly lower than ours for red galaxies, but agree for blue galaxies. Differences in modelling and/or in stellar mass estimates may be at least partly responsible for these differences, which in any case are not very statistically significant.

The lower-left panel of Fig. 12 shows a comparison with two rather different results. More et al. (2011) used satellite kinematics of central galaxies to infer the relation between halo and stellar mass. Their results agree with ours at high mass, but are significantly higher for $M_*^{\rm (MPA)} < 10^{11}\,{\rm M}_\odot$ (however, at the lowest masses the discrepancy is not significant, primarily due to our much larger errors). One possible explanation for a discrepancy of this sign is satellite contamination of their central galaxy sample (Skibba et al. 2011; Lin et al. 2015), which could be more important below $M_* \sim 10^{11}\,{\rm M}_\odot$; however, More et al. (2011) applied additional isolation criteria to avoid this problem. There are slight differences in their sample selection due to their different isolation criterion and colour cuts, though it is unclear why those would cause a difference that always goes in the same direction. The most likely remaining

[6] Also, for red galaxies, increasing the concentration by 35 per cent results in notably worse χ^2 values; the data in fact prefer *reduced* concentrations rather than increased ones. For blue galaxies, there is less discriminating power between concentrations due to the lower S/N.

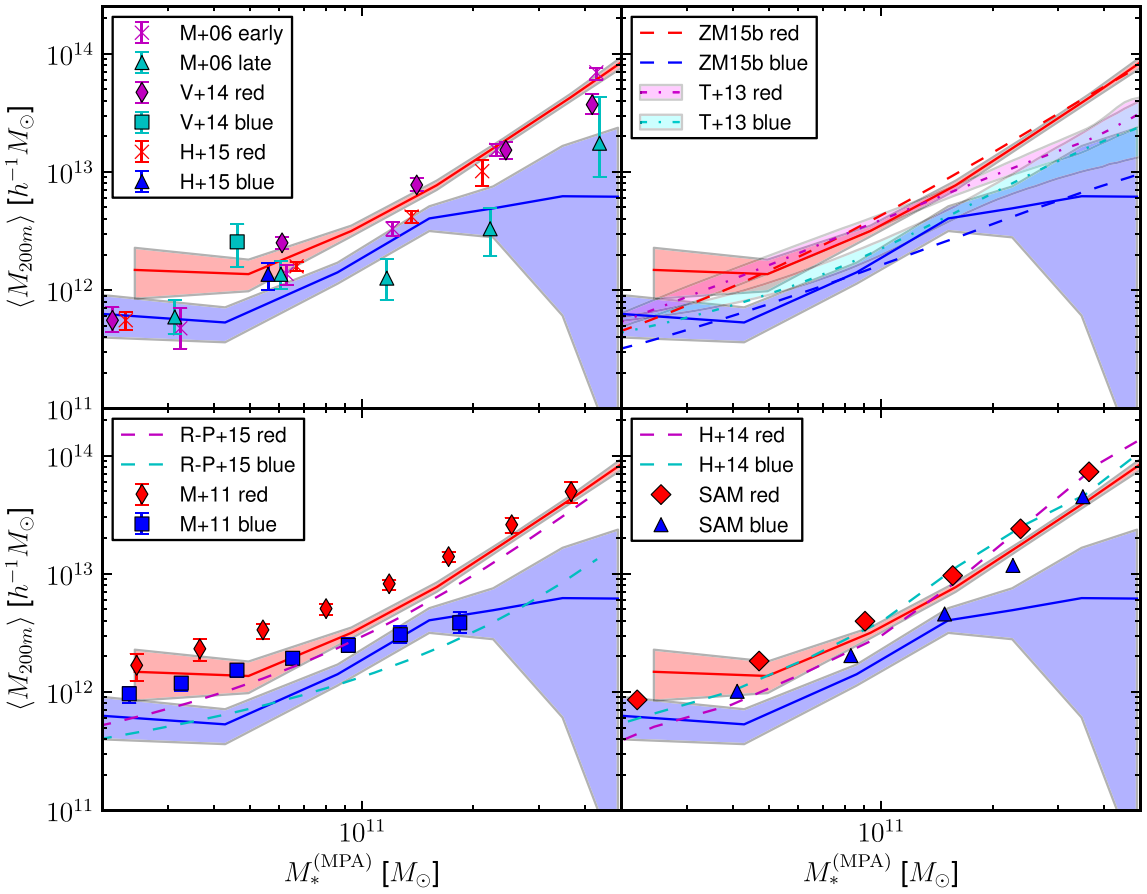

Figure 12. All panels show the mean central halo mass as a function of stellar mass for red and blue galaxies from this paper (Fig. 11) as shaded regions. The top-left panel shows results from measurements of galaxy–galaxy lensing by Mandelbaum et al. (2006), Velander et al. (2014) and Hudson et al. (2015); the bottom-left panel shows results from More et al. (2011, satellite kinematics) and Rodríguez-Puebla et al. (2015, HOD interpretation of abundance and clustering); the top-right panel shows results from HOD modelling of lensing and clustering measurements by Zu & Mandelbaum (2015a) and Tinker et al. (2013); and the bottom-right panel shows age-matching mocks from Hearin et al. (2014) as well as the semi-analytic catalogues used throughout this work. All errors are 1σ.

explanations are modelling issues that may be more relevant at lower mass, where the number of satellites per halo becomes quite small on average; we defer further exploration to future work. For a comparison of several kinematics-based stellar versus halo mass relations, see Wojtak & Mamon (2013).

Also in the lower panel of Fig. 12 are the results of Rodríguez-Puebla et al. (2015), who used a halo occupation distribution (HOD) to interpret the stellar mass function and galaxy clustering of low-redshift galaxies in the SDSS. We show their mean halo mass as a function of stellar mass without error bars, since the errors are very small compared to ours. Their results agree fairly well with ours for blue galaxies, but are below our results for red galaxies above $10^{11}\,\mathrm{M}_\odot$. It is possible that in the absence of lensing, their halo masses are more reliant on assumptions within their halo model to interpret the clustering. Wang et al. (2016) show that even with the same cosmological model and stellar mass function, the clustering signal can vary significantly depending on model assumptions. We propose that this may be the primary cause for the discrepancy.

The top-right panel of Fig. 12 includes two papers that interpreted galaxy–galaxy lensing and clustering measurements jointly. The results of Zu & Mandelbaum (2015a) were obtained by applying a halo model to the galaxy–galaxy lensing and clustering measurements of Main sample galaxies divided by colour and stellar mass (i.e. data similar to the 'Main sample' curves in Figs 8 and 9). As shown, these agree extremely well with our LBG results, despite the significantly more complex modelling needed to interpret those results. The halo model used there must account for the contributions by those Main sample galaxies that are satellites, and includes the effects of scatter between stellar and halo mass. The fact that our results are consistent with theirs after using our mock-catalogue-based correction for that scatter in the LBG signals is a non-trivial result.

The curves from Tinker et al. (2013) in the top-right panel of Fig. 12 were obtained by jointly modelling the stellar mass function, lensing and clustering in the COSMOS survey using a formalism that essentially doubles the number of halo model parameters in order to separately describe the results for red and blue galaxies. As shown, for blue galaxies their results are consistently slightly above ours, but with significant overlap of the error regions. For red galaxies, their results are consistent with ours for $M_* < 10^{11}\,\mathrm{M}_\odot$, but deviate to significantly lower halo masses at high stellar mass. As a consequence of these two differences, the red versus blue halo mass difference inferred from their results is smaller than ours. At the higher mass end, it is likely that their results are dominated by the higher S/N stellar mass function and clustering constraints, which may be more dependent on modelling assumptions as mentioned above in the discussion of the Rodríguez-Puebla et al. (2015) results. It is also worth noting that the mean redshift for this result is 0.36, so there may be some small evolutionary effects complicating the comparison between their results and ours.

Finally, the bottom-right panel of Fig. 12 shows the results of two mock catalogues. The first are the age-matching (Hearin & Watson 2013) mock catalogues publicly released with Hearin et al. (2014), who used stellar mass rather than luminosity as in the original age-matching paper. We show the mean halo mass at fixed stellar mass without error bars, since the error on the mean is quite small. As shown, the $\langle M_{200m}\rangle$ curve for red central galaxies is slightly steeper than in our LBG results. However, as a basic consequence of their age-matching procedure, their $\langle M_{200m}\rangle$ for blue central galaxies are above the red ones for much of the stellar mass range. This results in a highly significant discrepancy with our observations of blue central galaxy halo masses. The inversion of the red and blue curves over a wide range of stellar mass, which results from the assumptions of the method and some particular implementation details in Hearin et al. (2014), is discussed in more detail in Zu & Mandelbaum (2015a). It is worth noting, however, that Hearin et al. (2014) explored their ability to predict observable quantities associated with mixed galaxy samples containing central and satellite galaxies. In principle, a cancellation between effects seen in the two samples could be removed when exploring a sample of purely central galaxies, giving a more severe discrepancy with observations in our work compared to the moderate tension shown in the plots in Hearin et al. (2014). As mentioned in Section 2.1, the fact that our sample is not volume limited [and the one used by Hearin et al. (2014) is volume limited] cannot be responsible for these differences. A direct comparison of the $\Delta\Sigma$ profiles for all Main sample galaxies, and for LBGs, against predictions from the Hearin et al. (2014) is shown in Appendix C.

The points shown in the bottom-right panel of Fig. 12 are from the central galaxies in the semi-analytic mock catalogues used throughout this work (Section 3), using the same set of stellar mass bins as for the data. The statistical errors on the mean masses are not shown because they are very small; the systematic uncertainties are larger (Section 5.3). As shown, the curves for red central galaxies in the SAM-based catalogues are slightly above our observations, but not in a significant way except for at $M_* > 10^{11.2}\,\mathrm{M}_\odot$, also reflected in Fig. 10. The deviation between our observations and the blue galaxy halo masses in the mocks is also more significant at the highest stellar masses ($>10^{11}\,\mathrm{M}_\odot$) where we have very few galaxies. Overall, the mock catalogues exhibit a difference between the average halo masses for red and blue central galaxies in these bins that is consistently of the correct sign and slightly smaller magnitude compared to the real data. This is remarkable since no clustering or lensing information was used when tuning the parameters controlling formation and quenching processes in this simulation.

From a theoretical standpoint, it is interesting to consider how our results can be used. For example, the upper-right panel of Fig. 12 shows a comparison against a halo model that includes a prescription for quenching (the shutdown of star formation activity that transforms a galaxy from active to passive) from Zu & Mandelbaum (2015a) and matches our results very well. This quenching model, necessary to make a colour-dependent HOD, adds four parameters to the halo model, which is much fewer than the most obvious way to make a colour-dependent HOD (which would double the number of parameters). Different models for the quenching process – i.e. different dependences on stellar and/or halo mass – modify the mean halo mass at fixed stellar mass, suggesting that one can use our central galaxy constraints from this paper to constrain quenching models. In contrast, the poor match to the average halo masses in the age-matching mocks from Hearin et al. (2014) calls into question the assumptions underlying the galaxy–dark matter connection in those mock catalogues.

6 DISCUSSION AND CONCLUSIONS

In this work, we have used the galaxy–galaxy lensing signals of a sample of LBGs in the SDSS Main galaxy sample to measure the mean dark matter halo masses for central galaxies as a function of their stellar mass and colour. To validate the relatively simple interpretation of these lensing signals in terms of average halo masses, we have used both simulation-based mock catalogues that closely reproduce the observed properties of Main sample galaxies and LBGs, and cross-checks within the observational data set itself. We observe a clear, $>3\sigma$ difference in the average halo masses of blue and red central galaxies at fixed stellar mass, for all stellar masses above $6 \times 10^{10}\,\mathrm{M}_\odot$. The halo masses of the red (passive) central galaxies are higher than those of blue (active) central galaxies. We have demonstrated that selection effects cannot be responsible for this result, using a semi-analytic mock catalogue that reproduces many properties of the LBG sample.

Our result that there is a bimodality in halo masses of central galaxies at fixed stellar mass can be related to the underlying physical processes such as feedback. For example, Wang & White (2012) used indirect measures of halo mass (the satellite counts around central galaxies) to infer a difference in average halo mass at fixed stellar mass for isolated red and blue primary galaxies. Their finding in a mock catalogue that exhibited the similar effect (Guo et al. 2011) was that this could be attributed to AGN feedback suppressing star formation in central galaxies that have massive black holes, thus lowering the average stellar mass for red galaxies at fixed halo mass (or, at fixed stellar mass, giving a larger average halo mass for red primaries than for blue ones).

As discussed in Section 5.4, our results are largely consistent with previous lensing results (Mandelbaum et al. 2006; Velander et al. 2014; Hudson et al. 2015), with only minor tensions that may result from different modelling processes, stellar mass estimates, or ways of dividing the sample into blue and red subsets. We observe a clear tension with the results from satellite kinematics (More et al. 2011) below $M_* = 10^{11}\,\mathrm{M}_\odot$, likely due to modelling differences. Our tension goes in the same direction for both the red and blue samples, with the kinematics results giving a higher mass; thus, our work and theirs come to the same basic conclusion that red galaxy samples have higher average halo masses than blue galaxy samples at fixed stellar masses. Our results for blue galaxies are consistent with those of Rodríguez-Puebla et al. (2015), who used an HOD model to interpret galaxy clustering and the stellar mass function, but our results for red galaxies are in disagreement with theirs, likely due to the increased sensitivity to modelling assumptions when using clustering to infer halo masses. However, our results are consistent with those based on HOD modelling of galaxy–galaxy lensing and clustering by Zu & Mandelbaum (2015a) using a formalism that incorporates the results of halo quenching. We also observe a highly significant disagreement with the blue central galaxy halo masses in the age-matching mocks from Hearin et al. (2014), due to an inversion in those mocks of the average halo masses for red and blue central galaxies.

Our results clearly imply that high-fidelity mock catalogues that reproduce the galaxy–matter connection cannot be produced using methods that neglect type dependence, such as simple halo modelling. In addition, the age-matching approach appears to give average halo masses for blue central galaxies that are highly discrepant with our observations, as discussed in more depth in Section 5.4. More sophisticated methods that include a strong galaxy type dependence in $\langle M_{200m}\rangle$ (enforcing the correct sign of the difference) at fixed stellar mass seem to be necessary to reproduce

observations; as we have demonstrated, this can be achieved with SAMs or a type-dependent halo model.

ACKNOWLEDGEMENTS

The authors thank Jeremy Tinker for providing the curves from Tinker et al. (2013) shown in Fig. 12, and the anonymous referee for suggestions that improved the presentation of results in this work. RM and YZ acknowledge the support of the Alfred P. Sloan Foundation. WW acknowledges a Durham Junior Research Fellowship (RF040353). BH and SW were supported in part by the Advanced Grant 246797 'GALFORMOD' from the European Research Council, and BH by a Zwicky fellowship. SM is supported by World Premier International Research Center Initiative (WPI Initiative), MEXT, Japan, by the FIRST programme 'Subaru Measurements of Images and Redshifts (SuMIRe)', CSTP, Japan, and by Grants-in-Aid for Scientific Research from the JSPS Promotion of Science (No. 15K17600).

REFERENCES

Abazajian K. N. et al., 2009, ApJS, 182, 543
Aihara H. et al., 2011, ApJS, 193, 29
Anderson M. E., Gaspari M., White S. D. M., Wang W., Dai X., 2015, MNRAS, 449, 3806
Angulo R. E., Hilbert S., 2015, MNRAS, 448, 364
Angulo R. E., White S. D. M., 2010, MNRAS, 405, 143
Behroozi P. S., Conroy C., Wechsler R. H., 2010, ApJ, 717, 379
Bell E. F., de Jong R. S., 2001, ApJ, 550, 212
Benson A. J., 2012, New Astron., 17, 175
Bernstein G. M., Jarvis M., 2002, AJ, 123, 583
Blanton M. R., Roweis S., 2007, AJ, 133, 734
Blanton M. R. et al., 2005, AJ, 129, 2562
Bruzual G., Charlot S., 2003, MNRAS, 344, 1000
Cacciato M., van den Bosch F. C., More S., Li R., Mo H. J., Yang X., 2009, MNRAS, 394, 929
Cacciato M., van den Bosch F. C., More S., Mo H., Yang X., 2013, MNRAS, 430, 767
Chabrier G., 2003, PASP, 115, 763
Conroy C. et al., 2007, ApJ, 654, 153
Coupon J. et al., 2012, A&A, 542, A5
Coupon J. et al., 2015, MNRAS, 449, 1352
Cunha C. E., Lima M., Oyaizu H., Frieman J., Lin H., 2009, MNRAS, 396, 2379
Diemer B., Kravtsov A. V., 2015, ApJ, 799, 108
Eisenstein D. J. et al., 2001, AJ, 122, 2267
Feldmann R. et al., 2006, MNRAS, 372, 565
Fukugita M., Ichikawa T., Gunn J. E., Doi M., Shimasaku K., Schneider D. P., 1996, AJ, 111, 1748
Gunn J. E. et al., 1998, AJ, 116, 3040
Guo Q., White S., Li C., Boylan-Kolchin M., 2010, MNRAS, 404, 1111
Guo Q. et al., 2011, MNRAS, 413, 101
Han J. et al., 2015, MNRAS, 446, 1356
Hearin A. P., Watson D. F., 2013, MNRAS, 435, 1313
Hearin A. P., Watson D. F., Becker M. R., Reyes R., Berlind A. A., Zentner A. R., 2014, MNRAS, 444, 729
Henriques B. M. B., White S. D. M., Thomas P. A., Angulo R., Guo Q., Lemson G., Springel V., Overzier R., 2015, MNRAS, 451, 2663
Heymans C. et al., 2006, MNRAS, 371, L60
Hirata C., Seljak U., 2003, MNRAS, 343, 459
Hoekstra H., Yee H. K. C., Gladders M. D., 2004, ApJ, 606, 67
Hoekstra H., Hsieh B. C., Yee H. K. C., Lin H., Gladders M. D., 2005, ApJ, 635, 73
Hogg D. W., Finkbeiner D. P., Schlegel D. J., Gunn J. E., 2001, AJ, 122, 2129
Hoshino H. et al., 2015, MNRAS, 452, 998
Hudson M. J. et al., 2015, MNRAS, 447, 298
Ivezić Ž. et al., 2004, Astron. Nachr., 325, 583
Kauffmann G., Nusser A., Steinmetz M., 1997, MNRAS, 286, 795
Kauffmann G. et al., 2003, MNRAS, 341, 33
Khandai N., Di Matteo T., Croft R., Wilkins S., Feng Y., Tucker E., DeGraf C., Liu M.-S., 2015, MNRAS, 450, 1349
Komatsu E. et al., 2011, ApJS, 192, 18
Leauthaud A. et al., 2012a, ApJ, 744, 159
Leauthaud A. et al., 2012b, ApJ, 746, 95
Li C., White S. D. M., 2009, MNRAS, 398, 2177
Lin Y.-T., Mandelbaum R., Huang Y.-H., Huang H.-J., Dalal N., Diemer B., Jian H.-Y., Kravtsov A., 2015, ApJ, preprint (arXiv:1504.07632)
Lupton R. H., Gunn J. E., Ivezić Z., Knapp G. R., Kent S., Yasuda N., 2001, in Harnden F. R., Jr, Primini F. A., Payne H. E., eds, ASP Conf. Ser. Vol. 238, Astronomical Data Analysis Software and Systems X. Astron. Soc. Pac., San Francisco, p. 269
Mandelbaum R. et al., 2005a, MNRAS, 361, 1287
Mandelbaum R., Tasitsiomi A., Seljak U., Kravtsov A. V., Wechsler R. H., 2005b, MNRAS, 362, 1451
Mandelbaum R., Seljak U., Kauffmann G., Hirata C. M., Brinkmann J., 2006, MNRAS, 368, 715
Mandelbaum R., Seljak U., Baldauf T., Smith R. E., 2010, MNRAS, 405, 2078
Mandelbaum R., Hirata C. M., Leauthaud A., Massey R. J., Rhodes J., 2012, MNRAS, 420, 1518
Mandelbaum R., Slosar A., Baldauf T., Seljak U., Hirata C. M., Nakajima R., Reyes R., Smith R. E., 2013, MNRAS, 432, 1544
Miyatake H. et al., 2015, ApJ, 806, 1
More S., van den Bosch F. C., Cacciato M., Mo H. J., Yang X., Li R., 2009, MNRAS, 392, 801
More S., van den Bosch F. C., Cacciato M., Skibba R., Mo H. J., Yang X., 2011, MNRAS, 410, 210
More S., Miyatake H., Mandelbaum R., Takada M., Spergel D. N., Brownstein J. R., Schneider D. P., 2015, ApJ, 806, 2
Moster B. P., Somerville R. S., Maulbetsch C., van den Bosch F. C., Macciò A. V., Naab T., Oser L., 2010, ApJ, 710, 903
Nakajima R., Mandelbaum R., Seljak U., Cohn J. D., Reyes R., Cool R., 2012, MNRAS, 420, 3240
Navarro J. F., Frenk C. S., White S. D. M., 1997, ApJ, 490, 493
Padmanabhan N. et al., 2008, ApJ, 674, 1217
Parejko J. K. et al., 2013, MNRAS, 429, 98
Pier J. R., Munn J. A., Hindsley R. B., Hennessy G. S., Kent S. M., Lupton R. H., Ivezić Ž., 2003, AJ, 125, 1559
Planck Collaboration XI, 2013, A&A, 557, A52
Planck Collaboration XVI, 2014, A&A, 571, A16
Reyes R., Mandelbaum R., Gunn J. E., Nakajima R., Seljak U., Hirata C. M., 2012, MNRAS, 425, 2610
Richards G. T. et al., 2002, AJ, 123, 2945
Rodríguez-Puebla A., Avila-Reese V., Yang X., Foucaud S., Drory N., Jing Y. P., 2015, ApJ, 799, 130
Schaye J. et al., 2015, MNRAS, 446, 521
Skibba R. A., van den Bosch F. C., Yang X., More S., Mo H., Fontanot F., 2011, MNRAS, 410, 417
Smith J. A. et al., 2002, AJ, 123, 2121
Spergel D. N. et al., 2003, ApJS, 148, 175
Springel V. et al., 2005, Nature, 435, 629
Strauss M. A. et al., 2002, AJ, 124, 1810
Tinker J. L., Leauthaud A., Bundy K., George M. R., Behroozi P., Massey R., Rhodes J., Wechsler R. H., 2013, ApJ, 778, 93
Tucker D. L. et al., 2006, Astron. Nachr., 327, 821
van Uitert E., Cacciato M., Hoekstra H., Herbonnet R., 2015, A&A, 579, A26
Velander M. et al., 2014, MNRAS, 437, 2111
Vogelsberger M. et al., 2014, Nature, 509, 177
Wang W., White S. D. M., 2012, MNRAS, 424, 2574
Wang W., Sales L. V., Henriques B. M. B., White S. D. M., 2014, MNRAS, 442, 1363

Wang W., White S. D. M., Mandelbaum R., Henriques B., Anderson M. E., Han J., 2016, MNRAS, 456, 2301
Wechsler R. H., Bullock J. S., Primack J. R., Kravtsov A. V., Dekel A., 2002, ApJ, 568, 52
White M. et al., 2011, ApJ, 728, 126
Wojtak R., Mamon G. A., 2013, MNRAS, 428, 2407
York D. G. et al., 2000, AJ, 120, 1579
Zehavi I. et al., 2005, ApJ, 630, 1
Zehavi I. et al., 2011, ApJ, 736, 59
Zu Y., Mandelbaum R., 2015a, preprint (arXiv:1509.06758)
Zu Y., Mandelbaum R., 2015b, MNRAS, 454, 1161

APPENDIX A: TESTS OF THE NON-VOLUME-LIMITED NATURE OF THE SAMPLE

As described in Section 2.1, we compared the lensing signals for the full LBG samples (as shown in Fig. 7) with those for the LBGs at $z < 0.08$. While technically the redshift below which the samples are volume limited depends on the stellar mass range, this serves as an approximate test for how much it matters that the samples are not volume limited. Fig. A1 compares the lensing signals for the red

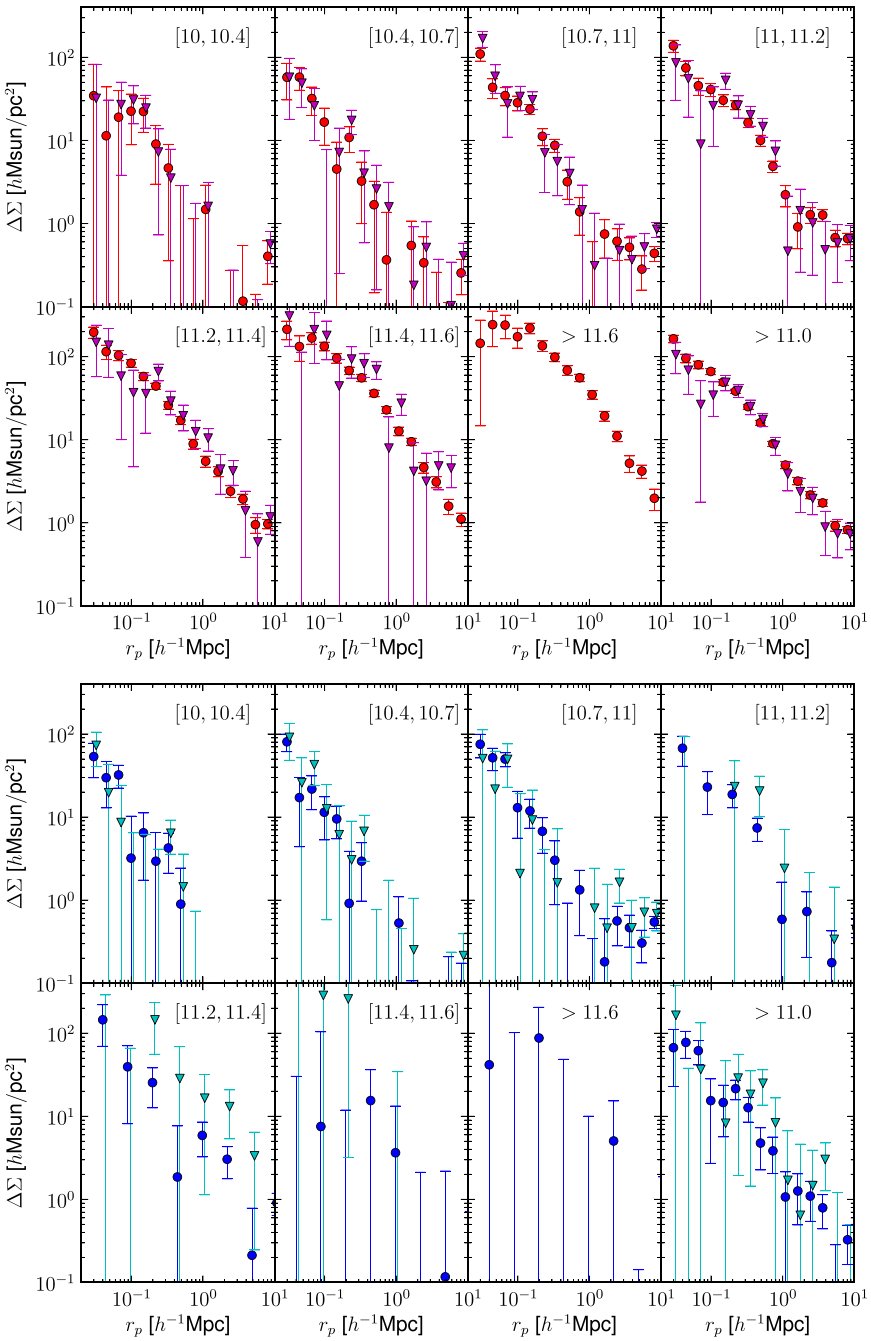

Figure A1. Comparison between lensing signals for all LBGs and for $z < 0.08$ LBGs for the red (top) and blue (bottom) subsamples, split into the same stellar mass bins as in the rest of this paper. The data for all LBGs are the same as in Fig. 7. In both panels, the circles (triangles) show the results for LBGs ($z < 0.08$ LBGs). Neither panel has $z < 0.08$ LBG results for the highest stellar mass sample, just because there are almost no lenses in that sample below that redshift.

Table B1. Summary of our results for the average halo mass for central galaxies in fixed stellar mass bins for red (top section) and blue (bottom section) central galaxies. The quantities that are tabulated are the lensing-weighted stellar mass of the galaxies taking into account their weight in the lensing measurement for our canonical (VAGC) stellar masses as well as for the MPA/JHU stellar masses, the mean halo mass, the ratio of central stellar mass to host halo mass normalized by Ω_b/Ω_m assuming a Planck Collaboration XVI (2014) cosmology for the VAGC and MPA/JHU stellar masses, respectively, and finally the multiplicative correction factor used to estimate the mean halo mass for central galaxies from the best-fitting NFW mass.

$\log_{10}\left(\frac{M_{*,\rm eff}}{\rm M_\odot}\right)$	$\log_{10}\left(\frac{M^{\rm MPA}_{*,\rm eff}}{\rm M_\odot}\right)$	$\log_{10}\left(\frac{\langle M_{200m}\rangle}{h^{-1}\,\rm M_\odot}\right)$	$\frac{M_{*,\rm cen}/M_{200m}}{\Omega_b/\Omega_m}$	$\frac{M^{\rm MPA}_{*,\rm cen}/M_{200m}}{\Omega_b/\Omega_m}$	$\frac{M_{200m}}{M^{\rm (uncorr)}_{200m}}$
		Red			
10.28	10.39	$12.17^{+0.19}_{-0.24}$	$0.056^{+0.042}_{-0.020}$	$0.072^{+0.054}_{-0.025}$	1.22
10.58	10.70	$12.14^{+0.12}_{-0.14}$	$0.121^{+0.048}_{-0.030}$	$0.158^{+0.062}_{-0.039}$	1.36
10.86	10.97	$12.50^{+0.04}_{-0.05}$	$0.100^{+0.011}_{-0.010}$	$0.129^{+0.014}_{-0.013}$	1.38
11.10	11.20	$12.89^{+0.04}_{-0.04}$	$0.071^{+0.007}_{-0.006}$	$0.090^{+0.009}_{-0.008}$	1.37
11.29	11.38	$13.25^{+0.03}_{-0.03}$	$0.047^{+0.004}_{-0.003}$	$0.058^{+0.004}_{-0.003}$	1.31
11.48	11.56	$13.63^{+0.03}_{-0.03}$	$0.031^{+0.002}_{-0.002}$	$0.037^{+0.003}_{-0.002}$	1.16
11.68	11.75	$14.05^{+0.05}_{-0.05}$	$0.019^{+0.002}_{-0.002}$	$0.022^{+0.003}_{-0.002}$	1.06
		Blue			
10.24	10.29	$11.80^{+0.16}_{-0.20}$	$0.120^{+0.070}_{-0.037}$	$0.134^{+0.078}_{-0.041}$	1.09
10.56	10.63	$11.73^{+0.13}_{-0.17}$	$0.297^{+0.140}_{-0.076}$	$0.351^{+0.165}_{-0.089}$	1.11
10.85	10.94	$12.15^{+0.08}_{-0.10}$	$0.218^{+0.054}_{-0.037}$	$0.265^{+0.065}_{-0.046}$	1.18
11.10	11.18	$12.61^{+0.10}_{-0.11}$	$0.136^{+0.038}_{-0.028}$	$0.164^{+0.045}_{-0.034}$	1.29
11.28	11.35	$12.69^{+0.19}_{-0.25}$	$0.169^{+0.128}_{-0.059}$	$0.200^{+0.152}_{-0.070}$	1.45
11.47	11.54	$12.79^{+0.43}_{-1.01}$	$0.206^{+1.908}_{-0.129}$	$0.243^{+2.247}_{-0.152}$	1.42
11.68	11.69	$12.79^{+0.58}_{-2.23}$	$0.338^{+57.069}_{-0.250}$	$0.346^{+58.399}_{-0.256}$	1.57

(top) and blue (bottom) LBGs with those for $z < 0.08$ LBGs. The results are fully consistent with each other, supporting our choice to proceed with the full LBG samples.

APPENDIX B: MASS RESULTS

In Table B1, we summarize our average halo mass results and other relevant statistics for red (top section) and blue (bottom section) central galaxies. The error bars on the mean halo masses are actually the 16th and 84th percentile values of the non-Gaussian error distribution. We have used those same percentile values to give non-Gaussian 16th and 84th percentile values for the ratio of stellar-to-halo mass (normalized by Ω_b/Ω_m). Finally, the total corrections applied to the NFW masses, including the effects of completeness and impurity of the LBG sample as well as systematics in the fitting (e.g. due to the finite width of the halo mass distribution), are shown as the last column. These are the product of the two correction factors derived in Section 3.

APPENDIX C: AGE-MATCHING COMPARISON IN DETAIL

In this appendix, we present the results of comparing $\Delta\Sigma$ profiles in the $z = 0$ catalogue provided by Hearin et al. (2014) with the observed $\Delta\Sigma$ profiles for red and blue LBGs and Main sample galaxies in this work. This comparison avoids the mass inference procedure, and depends simply on replicating the LBG selection in those mock catalogues. While we use the $z = 0$ simulation snapshot, we weight the LBGs to reproduce the lensing-weighted stellar mass distribution in the observed (flux-limited) LBG sample.

The results of the $\Delta\Sigma$ comparison are shown in Fig. C1. Since our samples are not at $z = 0$, we must make a choice as to whether we take the $\Delta\Sigma$ profiles in their $z = 0$ simulation as being in physical separations, so no conversion is done to account for the differences in redshift, or whether their predictions are in comoving coordinates, requiring a conversion to compare with our results. We show both options in this figure, but the difference between them is not sufficient to substantially change our conclusions.

As shown, for red galaxies, the age-matching predictions are only mildly discrepant with the data. At high mass, the mocks predict significantly higher concentrations for red galaxies than are suggested by the observed $\Delta\Sigma$ profiles in the real data. The discrepancies between the model and data are particularly evident for the higher mass blue galaxies (middle and right-hand panels), similar to the results shown in Fig. 12 when comparing masses. It is interesting to note that for $M_* < 10^{11}\,\rm M_\odot$, the blue masses are higher than the red ones in Fig. 12, but this is not strongly reflected in the $\Delta\Sigma$ profiles for LBGs. This is primarily due to the fact that the model also includes a segregation of the red and blue into haloes of different concentrations, resulting in profile differences that partly counteract the effect of the mass differences and result in the red profiles being above the blue for $r_p \lesssim 0.2\,h^{-1}$ Mpc (and the opposite is true for larger r_p). For $M_* > 10^{11}\,\rm M_\odot$, Fig. 12 shows that the red galaxies have higher halo masses than the blue ones, and this is reflected in the $\Delta\Sigma$ profiles; however, the $\Delta\Sigma$ profiles for the blue LBGs (or all galaxies) are well above the data in this bin.

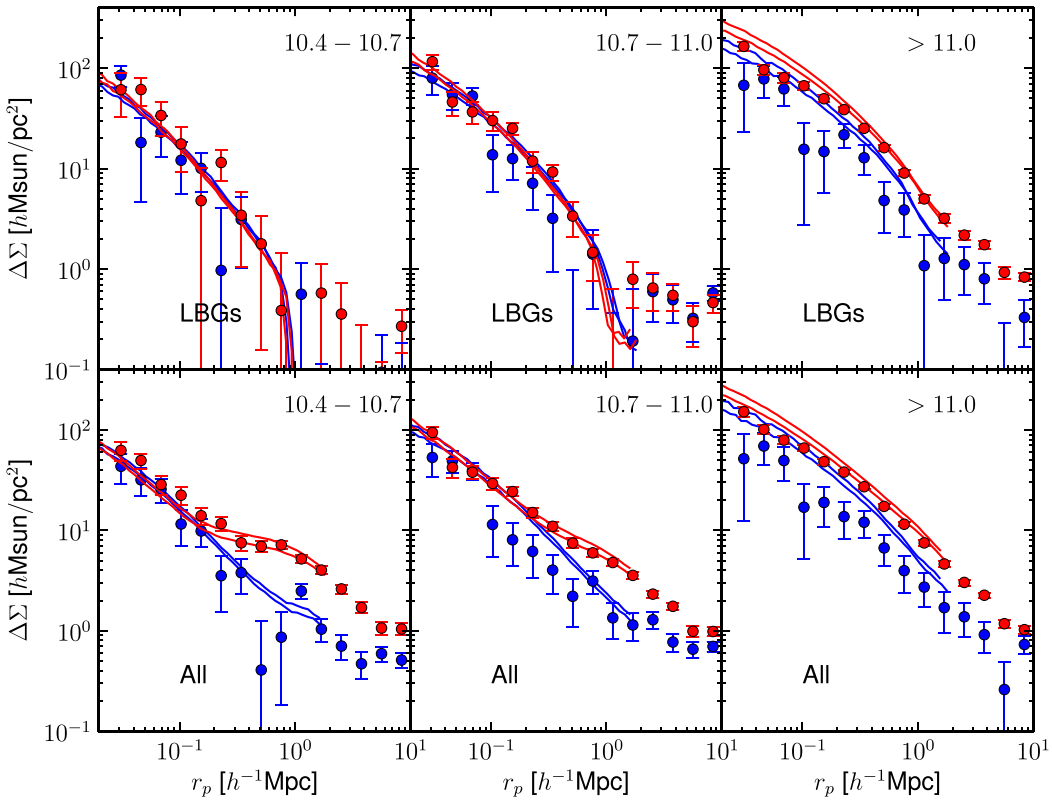

Figure C1. Points with error bars show lensing signals for red and blue LBGs (top) and Main sample galaxies without LBG selection (bottom) in stellar mass bins. The lines show the predictions from the Hearin et al. (2014) age-matching mock catalogues, with two lines for each sample (depending on whether we treat their predictions as being fixed in physical or comoving coordinates, with the latter always being higher than the former).

This paper has been typeset from a TEX/LATEX file prepared by the author.